UNIVERSITÄT BONN
Physikalisches Institut

Calculation of the Polarization Observables of the radiative capture $d + p \to {}^3He + \gamma$

by

Omid Nohadani

The vector and tensor polarization observables of the capture reaction $d + p \to {}^3He + \gamma$ are calculated for energies up to 100 MeV within the framework of coupled integral equations employing separable versions of the Paris, the Bonn-A, and Bonn-B potentials. The Ernst-Shakin-Thaler (EST) approximation is used for the separable representation of the two-body inputs in the Alt-Grassberger-Sandhas (AGS) three-nucleon equations. In the calculations Mesonic exchange currents, final state interaction, and $E2$-contributions are taken into account, which are necessary for a good agreement between theory and experiment.

Post address:
Nussallee 12
53115 Bonn
Germany

BONN-IB-2000-04
Bonn University
January 2000

UNIVERSITÄT BONN
Physikalisches Institut

Berechnung von Polarisations-Observablen beim radioaktiven Einfang $d + p \rightarrow {}^3He + \gamma$

von

Omid Nohadani

Dieser Forschungsbericht wurde als Diplomarbeit von der
Mathematisch - Naturwissenschaftlichen Fakultät der Universität Bonn angenommen.

Angenommen am:	31. Januar 2000,
Referent:	Prof. Dr. W. Sandhas
Korreferent:	Prof. Dr. D. Schütte

Contents

1 Introduction

The investigation of the three-nucleon problem is of high importance for checking the quality of nuclear interactions. Realistic potentials are well adjusted to the experimental two-nucleon data, but they still do not provide all experimental three-nucleon data. Three-nucleon scattering calculations, thus, can point to the real nature of the nuclear forces. Of an also high interest are calculations of the three-nucleon photodisintegration or of the inverse radiative capture process. There the matrix elements contain the continuum states as well as the three-body bound states. Hence, they enable a better test of the nucleon-nucleon interaction than scattering and break-up calculations.

Technically, our calculations are based on the Faddeev-type AGS formalism [1], adjusted to photonuclear processes [2], as done already by Gibson and Lehman [3]. After separable expansion of the two-body potentials this momentum space formulation of the three-body problem – introduced by Alt, Grassberger and Sandhas – is most directly reduced to effective two-body equations. It is therefore particularly suitable for numerical treatments than, as will be shown in Section 2.

Detailed, highly accurate [4] calculations of the cross sections of photonuclear and radiative capture reactions of ^3H and ^3He were done by Schadow and Sandhas [5–8]. They show at low energies a pronounced potential dependence which, however, is to be contrasted with considerable experimental uncertainties. At higher energies the potential dependence vanishes, but the resulting theoretical curve lies between the two different data sets available. This situation and the big error bars call for new and more accurate measurements. Our goal in this work is to treat besides the differential cross section the vector and tensor polarization observables of the radiative capture reaction $p + d \rightarrow {}^3He + \gamma$ by using realistic nucleon-nucleon potentials. In fact, to get additional information on three-nucleon sensitivities, a detailed treatment of the polarization is necessary. Moreover, the spin distribution of the participating particles is not visible through the cross section measurements. Because of the discrepancy of the available realistic potentials concerning the triton binding energy, the calculated observables provide a further useful test of the employed potentials.

Calculations of different deuteron tensor analyzing powers of the capture reaction $^1H(\vec{d},\gamma)^3He$ at low energy ($E_d = 10$ MeV) have been done by Fonseca and Lehman [9]. There, the Paris two-nucleon interaction was used in the three-body equations and the electromagnetic transition is calculated with the Siegert $E1$ operator. They suggested to incorporate $E2$-contributions in order to clear up the occurring discrepancies between some of their calculations and the corresponding experimental data sets. Ishikawa and Sasakawa have calculated the tensor analyzing power A_{yy} by employing different choices of realistic potentials and including a three-nucleon potential [10].

The calculation of the original two-dimensional three-body scattering problem is nu-

merically quite demanding [11]. In order to reduce the complexity of the problem, it is, therefore, standard to expand the original non-separable potential into series of separable terms. The resulting one-dimensional integral equations are manageable with a considerably reduced computational effort.

Januschke has calculated polarization observables of the $n-d$ scattering for the Paris potential using the W-matrix representation of the two-body T-matrix [12]. There, the high quality of the W-matrix approach even for realistic nucleon-nucleon interactions is demonstrated.

In this work, we employ three different realistic potentials. These are the Paris [13], Bonn-A [14], and Bonn-B [15] potentials. We use for them the separable expansion developed by Ernst, Shakin, and Thaler (EST) [16,17]. This expansion of the mentioned potentials developed by the Graz group (PEST, BAEST, and BBEST) [18,19], have led to the first fully reliable realistic results in the three-nucleon problem [20,21]. In the following applications to photoprocess an improved parametrization by Haidenbauer is used [22]. Depending on the demanded accuracy one can choose for each partial wave different ranks of approximation, which increase the dimension of the system of equations.

The parametrization of the EST expansion of different potentials yields different binding energies. In Groningen [7] it was shown that the peak heights of the cross section calculations are correlated to the triton binding energy and that the chosen number of partial waves plays an crucial role, so that the peak heights for different potentials with the same number of partial waves lie on a straight line. In other words, the peak height does not appear as an independent observable. Most of the calculated polarization observables also do not show a significant dependence on the different realistic potentials. We notice, however, that it is not enough to employ only the Born-term , i.e., the inhomogeneity in the coupled integral equations. The incorporation of the final state interaction (FSI) by solving the whole set of equations is necessary, as observed in [5–7].

In Section 3, we show the role of meson exchange currents (MEC) taken into account by means of the Siegert theorem and electric multipoles $E1$ and $E2$. The numerical results are presented in Section 5. The transition matrices employed in this work are delivered by Schadow. As shown in Ref. [6,7], the asymmetry caused by the $E2$-contribution is necessary to describe the experimental data of the cross section. Our polarization calculations confirm this result. The dominance of the $E1$ transition is illustrated in Section 5 by various observables. There are still some discrepancies at the extreme forward and backward angles, which call for the calculation of $M1$-contributions.

2 The Three-Body Problem

The nonrelativistic quantum mechanical three-body problem has been widely studied over the last decades [3,20,21,23–32]. Using Faddeev-type coupled equations in momentum space which leads to the integral equations, we are able to investigate not only the bound states of a few-body system, but also the scattering of an elementary particle from a bound few-body system, in our case from a bound two-body system.

2.1 Notation and Kinematics

To describe the kinematic situation between three particles we introduce instead of the momenta $\vec{k}_i$ of each particle (corresponding to the coordinates in the momentum space) the total momentum

$$\vec{k} = \vec{k}_\alpha + \vec{k}_\beta + \vec{k}_\gamma \ , \tag{2.1}$$

the relative momentum in the (β, γ)-subsystem

$$\vec{p}_\alpha = \frac{m_\gamma \vec{k}_\gamma - m_\beta \vec{k}_\beta}{m_\gamma + m_\beta} , \tag{2.2}$$

and the momentum of the third free particle relative to the (β, γ)-subsystem

$$\vec{q}_\alpha = \frac{(m_\gamma + m_\beta)\vec{k}_\alpha - m_\alpha(\vec{k}_\beta + \vec{k}_\gamma)}{m_\alpha + m_\beta + m_\gamma} \ . \tag{2.3}$$

Note, that (α, β, γ) is a cyclic permutation of (1,2,3). In fact, $\vec{p}_\gamma$ becomes identical to $\vec{k}_\alpha$ in the center-of-mass-system (CMS) of particles α and β, while $\vec{q}_\gamma$ is equal to $\vec{k}_\gamma$ in the CMS of all three particles. Definitions (2.2) and (2.3) are illustrated in the following figure:

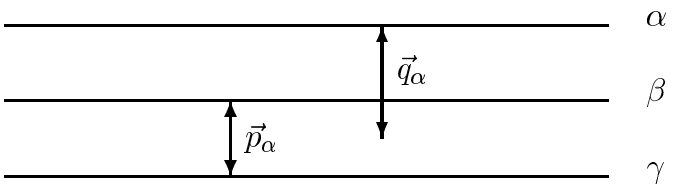

In the CMS of all three particles the total momentum $\vec{P} = \sum_i \vec{k}_i$ vanishes. The kinetic energy operator can be presented by these combinations instead of the original momenta

$\vec{k}_i$. If we restrict ourselves to a space spanned by the eigenvectors of the relative momentum operators, the full Hamiltonian is of the form,

$$H = \frac{q_\alpha^2}{2M_\alpha} + \frac{p_\alpha^2}{2\mu_\alpha} + \sum_\alpha V_\alpha = H_0 + \sum_\alpha V_\alpha \ , \tag{2.4}$$

where the potential $V = \sum_\gamma V_\gamma$ is chosen as a sum of two-body interactions $V_\gamma = V_{ij}$ with $\gamma \neq i,j$, operating in the two-body subsystem. Assuming translation invariance, the momentum-conserving δ-function is factored out in all subsequent relations. This, in particular, means that (2.4) acts on the plane waves $|\phi_{\vec{p}\alpha}\rangle$ and $|\phi_{\vec{q}\alpha}\rangle$ of particles $i,j \neq \alpha$ and of particle α relative to the (β,γ)-subsystem, respectively.
Furthermore, in (2.4) we used the reduced masses

$$\mu_\alpha = \frac{m_\beta m_\gamma}{m_\beta + m_\gamma} \qquad , \qquad M_\alpha = \frac{m_\alpha(m_\beta + m_\gamma)}{m_\alpha + m_\beta + m_\gamma} \ . \tag{2.5}$$

In the following it is important to differentiate between the two-body and three-body quantities. We will use a "hat" for the two-body quantities. If particle α is asymptotically free, the other two particles being bound, the channel Hamiltonian is given by

$$H_\alpha = \frac{q_\alpha^2}{2M_\alpha} + \frac{p_\alpha^2}{2\mu_\alpha} + V_\alpha = H_0 + V_\alpha \, . \tag{2.6}$$

Consequently, (2.6) is composed of the full two-body Hamiltonian

$$\hat{H}_\alpha = \frac{\hat{p}_\alpha^2}{2\mu_\alpha} + \hat{V}_\alpha \tag{2.7}$$

and the kinetic energy of the free particle. The eigenstates of H_α with $E_{\alpha n}$ as eigenvalues are the so-called channel states

$$|\phi_{\alpha n}\rangle = |\hat{\Psi}_{\alpha n}\rangle |\vec{q}_\alpha\rangle \, . \tag{2.8}$$

Since H_α now plays the role of the free Hamiltonian of particle α relative to the subsystem, the natural generalization of the Møller operator is the channel Møller operator

$$\Omega_\alpha^{(\pm)} = s - \lim_{t \to \mp\infty} e^{iHt} e^{-iH_\alpha t} \, . \tag{2.9}$$

By analogy with the general definition, channel scattering states are associated with the channel states (2.8),

$$|\hat{\Psi}_{\alpha n}^{(\pm)}\rangle = \Omega_\alpha^{(\pm)} |\phi_{\alpha n}\rangle \, . \tag{2.10}$$

2.2 AGS Equations

There are different kinds of scattering processes in the three-body case. We can prepare a system with an asymptotically free particle α moving relative to a bound two-body system (β, γ) as an initial state (2.8), which goes over into a final state

$$|\phi_{\beta m}\rangle = |\hat{\Psi}_{\beta m}\rangle |\vec{q}\,'_{\beta}\rangle \tag{2.11}$$

after the interaction. There are several options as illustrated in the following:

1. elastic scattering

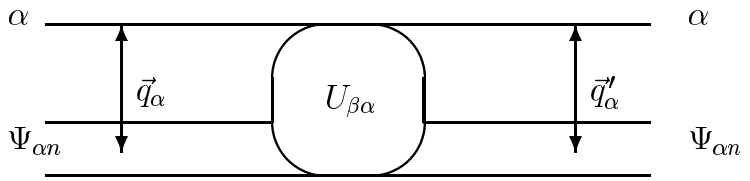

2. excitation

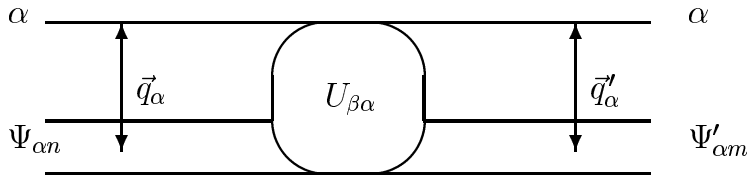

3. rearrangement

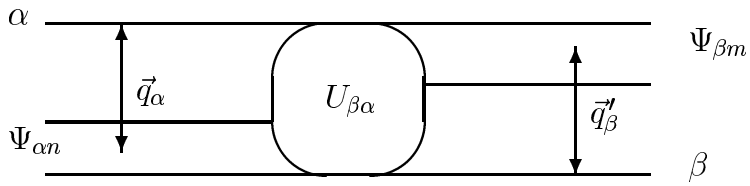

4. break-up

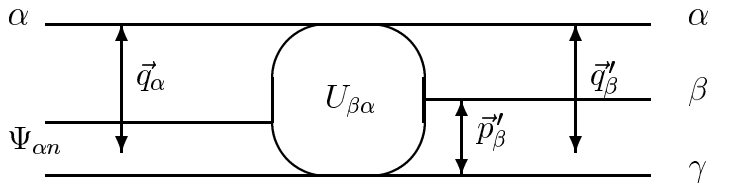

The break-up and excitation channels will not be considered in the following. To describe the illustrated transitions we need a set of transition operators $U_{\beta\alpha}$, which commonly depend on a complex energy variable z. Their on-shell matrix elements

$$\langle \vec{q}'_\beta | \langle \psi_{\beta m} | U_{\beta\alpha} | \psi_{\alpha n} \rangle | \vec{q}_\alpha \rangle \,, \tag{2.12}$$

build the input for the relation of observables. Introducing the resolvent of the full Hamiltonian

$$G(z) = (z - H)^{-1} \tag{2.13}$$

and the resolvent of H_0 ("the free Green's function")

$$G_0(z) = (z - H_0)^{-1} \tag{2.14}$$

to define the transition operator via

$$G(z) = \delta_{\beta\alpha} G_\alpha(z) + G_\beta(z) U_{\beta\alpha}(z) G_\alpha(z) \,, \tag{2.15}$$

to solve this special chosen $U_{\beta\alpha}(z)$, the so-called Alt-Grassberger- Sandhas (AGS) [1] equations

$$U_{\beta\alpha}(z) = \bar{\delta}_{\beta\alpha} G_0^{-1}(z) + \sum_\gamma \bar{\delta}_{\beta\gamma} T_\gamma(z) G_0(z) U_{\gamma\alpha}(z) \,, \tag{2.16}$$

with an anti-delta function, defined as

$$\bar{\delta}_{\beta\gamma} = 1 - \delta_{\beta\gamma} \,. \tag{2.17}$$

The advantage of this set of Faddeev-type equations is that they treat all channels simultaneously and yield, contrary to the channel specific Lippmann-Schwinger equations, z unique solutions for $z = E + i0$ [11]. This formulation of the three-body problem consists of an effective two-body equation and is therefore easily applicable for numerical treatments.

The potentials V_γ enter the AGS equations via the T-operator acting in the γ-subsystem

$$T_\gamma(z) = V_\gamma + V_\gamma G_\gamma(z) V_\gamma(z) \,. \tag{2.18}$$

The $T_\gamma(z)$ satisfy the two-body Lippmann-Schwinger equation

$$T_\gamma(z) = V_\gamma + V_\gamma G_0(z) T_\gamma(z) \,. \tag{2.19}$$

The three-body operators $T_\gamma(z)$ depend on the two-body operators $\hat{T}_\gamma(z)$ according to

$$\langle (\gamma) \vec{q}' \vec{p}' | T_\gamma(z) | (\gamma) \vec{q} \vec{p} \rangle = \delta(\vec{q}' - \vec{q}) \langle \vec{p}' | \hat{T}_\gamma(z - \frac{3}{4} q^2) | \vec{p} \rangle \,. \tag{2.20}$$

We see that the energy in the two-body subsystem is shifted by the kinetic energy of the third particle. Using the z-dependent operator valued matrices [11]

$$\begin{aligned} \mathbf{T}_{\beta\alpha} &= U_{\beta\alpha} \\ \mathbf{V}_{\beta\alpha} &= \bar{\delta}_{\beta\alpha} G_0^{-1} \\ \mathbf{G_0}_{,\beta\alpha} &= \delta_{\beta\alpha} G_0 T_\alpha G_0 \end{aligned} \tag{2.21}$$

the AGS equations (2.16) takes the Lippmann-Schwinger form

$$\mathbf{T} = \mathbf{V} + \mathbf{V}\,\mathbf{G_0}\,\mathbf{T}\,. \tag{2.22}$$

Now we can introduce – as in the two-body case – the resolvent

$$\mathbf{G} = \mathbf{G_0} + \mathbf{G_0}\,\mathbf{T}\,\mathbf{G_0} \tag{2.23}$$

and obtain

$$\mathbf{G} = \mathbf{G_0} + \mathbf{G_0}\,\mathbf{V}\,\mathbf{G}\,. \tag{2.24}$$

Comparing (2.23) and (2.24) yields the useful relationship

$$\mathbf{T}\,\mathbf{G_0} = \mathbf{V}\,\mathbf{G}\,, \tag{2.25}$$

known from the genuine two-body theory.

2.3 Transition amplitude

First, we discuss the transition amplitude of the triton photodisintegration. The equations we will derive can be used for describing radiative capture via time reversal invariance. The cross section for the two-body photodisintegration of triton is determined by the transition amplitude

$$^{(-)}\langle \Psi_\beta | H_{em} | \Psi_t \rangle\,, \tag{2.26}$$

with H_{em} being the electromagnetic interaction. The scattering state $|\Psi_\beta\rangle^{(-)\dagger}$ is defined (as above) with the channel state $|\Phi_\beta\rangle$ by

$$|\Psi_\beta\rangle^{(-)\dagger} = \lim_{\epsilon\to 0} -i\epsilon\, G(E_\beta - i\epsilon)\,|\Phi_\beta\rangle = \Omega_\beta^{(-)}\,|\Phi_\beta\rangle\,. \tag{2.27}$$

With the definition of the transition operators (2.15) the adjoint Møller operators read

$$\Omega_\beta^{(-)\dagger} = \delta_{\beta\alpha} + U_{\beta\alpha}(E_\beta + i0)\, G_\alpha(E_\beta + i0)\,. \tag{2.28}$$

Using equation (2.15) and the resolvent equation

$$G = G_\alpha + G_\alpha \bar{V}_\alpha G = G_\alpha + G \bar{V}_\alpha G_\alpha \,, \tag{2.29}$$

following from

$$G_\alpha^{-1} - G^{-1} = \bar{V}_\alpha \,, \tag{2.30}$$

one sees that the right-hand side of (2.28) depends only on α

$$\Omega_\beta^{(-)\dagger} = \delta_{\beta\alpha} + (G_\beta^{-1} G\, G_\alpha^{-1} - \delta_{\beta\alpha} G_\beta^{-1})\, G_\alpha = G_\beta^{-1}\, G = 1 + \bar{V}_\beta\, G \,. \tag{2.31}$$

We now multiply the AGS equations (2.16) with G_α and add $\delta_{\beta\alpha}$ to both sides

$$\begin{aligned} U_{\beta\alpha} G_\alpha + \delta_{\beta\alpha} &= \bar{\delta}_{\beta\alpha} G_0^{-1} G_\alpha + \delta_{\beta\alpha} + \sum_\gamma \bar{\delta}_{\beta\alpha} T_\gamma G_0 U_{\beta\alpha} G_\alpha \\ &= \bar{\delta}_{\beta\alpha} G_0^{-1} G_\alpha + \delta_{\beta\alpha} + \sum_\gamma \bar{\delta}_{\beta\alpha} T_\gamma G_0 (\Omega_\gamma^{(-)\dagger} - \delta_{\gamma\alpha}) \\ &= \bar{\delta}_{\beta\alpha} \underbrace{(G_0^{-1} G_\alpha - V_\alpha G_\alpha)}_{=1} + \delta_{\beta\alpha} + \sum_\gamma \bar{\delta}_{\beta\alpha} T_\gamma G_0 \Omega_\gamma^{(-)\dagger} \end{aligned} \tag{2.32}$$

in order to obtain an integral equation for the adjoint Møller operators (2.31):

$$\Omega_\beta^{(-)\dagger} = 1 + \sum_\gamma \bar{\delta}_{\beta\gamma} T_\gamma G_0 \Omega_\beta^{(-)\dagger} \,. \tag{2.33}$$

With these equations, one can write the transition amplitude of the two-body photodisintegration

$$\begin{aligned} & {}^{(-)}\langle \Psi_\beta | H_{em} | \Psi_t \rangle \\ = \;& \langle \Phi_\beta | \Omega_\beta^{(-)\dagger} H_{em} | \Psi_t \rangle \\ = \;& \underbrace{\langle \Phi_\beta | H_{em} | \Psi_t \rangle}_{\text{Born-term}} + \sum_\gamma \bar{\delta}_{\beta\gamma} \langle \Phi_\beta |\, T_\gamma(E + i0)\, G_0(E + i0) \Omega_\beta^{(-)\dagger} H_{em}\, | \Psi_t \rangle \,. \end{aligned} \tag{2.34}$$

The Born-term (conventionally called plane-wave approximation) characterizes the transition of the triton into a deuteron and a free neutron. The Born-term does not describe any interaction between these two outgoing particles. The final-state-interaction (FSI) is taken into account by solving the whole integral equation (2.34). The single Born-term represents only at high enough energies an acceptable approximation, because during the transfer of momentum the time of interaction is too short for an eventual rearrangement [5–7].

The three-body AGS equations are considerably simplified in separable approximation of T_γ. On of the most efficient separable extensions are developed by Ernst, Shakin and Thaler, the so-called EST-method [16,17]. This approach is described in Ref. [4].

2.3.1 Numerical handling

To solve an integral equation like the Lippmann-Schwinger equation, one has to reduce it to a linear equation [33]. The integral of such a partial wave integral equation like

$$T_l(k',k;E) = V_l(k',k) + \frac{2}{\pi}\int\limits_0^\infty dp \frac{p^2 V_l(k';p)\, T_l(p,k;E)}{E - E_p + i\epsilon} \tag{2.35}$$

has to be broken into principal-value and delta function parts, so that with the reduced mass

$$\mu = \frac{m_p\, m_d}{m_p + m_d} \tag{2.36}$$

this results in

$$\begin{aligned} T_l(k',k;E) = V_l(k',k) \;\; &+ \;\; \frac{2}{\pi}\int\limits_0^\infty dp\, \frac{p^2 V_l(k',p)\, T_l(p,k) - k_0^2\, V_l(k',k_0)\, T_l(k_0,k)}{(k_0^2 - p^2)/2\mu} \\ &- \;\; 2i\mu(k_0) k_0 V_l(k',k_0)\, T_l(k_0,k,E)\,, \end{aligned} \tag{2.37}$$

and after re-ordering, one obtains

$$\begin{aligned} T_l(k',k;E) \;\; &= \;\; V_l(k',k) + \frac{2}{\pi}\int\limits_0^\infty dp\, \frac{p^2 V_l(k',p)\, T_l(p,k)}{(k_0^2 - p^2)/2\mu} \\ &- \;\; \left\{ \frac{2}{\pi}\int\limits_0^\infty dp\, \frac{k_0^2}{(k_0^2 - p^2)/2\mu} + 2i\mu(k_0) k_0 \right\} V_l(k',k_0)\, T_l(k_0,k)\,. \end{aligned} \tag{2.38}$$

One can convert this integral equation into a set of linear equations by approximating the integral as a sum over N Gaussian quadrature points $k_j; j = 1, N$, each weighted by ω_j,

$$\begin{aligned} T_i(k',k;E) \;\; &= \;\; V_i + \frac{2}{\pi}\sum_{j=1}^{N} \frac{k_j^2 V_{ij} T_j \omega_j}{(k_0^2 - k_j^2)/2\mu} \\ &- \;\; \left\{ \frac{2}{\pi}\left(\sum_{m=1}^{N} \frac{\omega_m}{(k_0^2 - k_m^2)/2\mu} \right) k_0^2 + 2i\mu(k_0)\, k_0 \right\} V_{i0} T_0\,. \end{aligned} \tag{2.39}$$

The latter equation contains $N+1$ unknowns, $T(k_j,k_0)$ for $j = 1, N$ and $T(k_0,k_0)$. To solve it on-shell (i.e., $T(k_0,k_0)$) requires solving it for half-off-shell $T(k_j,k_0)$ for all k_j. This is done by evaluating the equation for k on a grid:

$$k_i = \begin{cases} k_j & \text{for} j = 1, N \text{ (quadrature points)}, \\ k_0 & \text{for} j = 0 \text{ (on-the-energy-shell-points)}. \end{cases} \tag{2.40}$$

Furthermore, to assist computing, one can express these equations as matrix equations by combining the energy denominators and weights into a single denominator function:

$$\tilde{D}_i = \begin{cases} \frac{2}{\pi} \cdot \frac{2\mu\omega_i k_i^2}{k_i^2 - k_0^2} & \text{for } i = 1 \cdots N \\ \left(-\frac{2}{\pi} \cdot 2\mu k_0^2 \sum_{j=1}^{N} \frac{\omega_i}{k_i^2 - k_0^2} \right) - 2\mu i k_0 & \text{for } i = N+1 \end{cases} \tag{2.41}$$

The reduction yields

$$V_i = T_i + \sum_{j=1}^{N} V_{ij} \tilde{D}_j T_j \,, \tag{2.42}$$

This linear equation is solvable by known numerical techniques.

2.4 Partial wave decomposition

For the numerical treatment of systems of equations as obtained in Section 2.3, we have to reduce their dimensions to a manageable size. By considering rotation invariance along the $\vec{z}$-axis (along the direction of the incoming particle), we can employ the corresponding partial wave decomposition. For this purpose we choose an appropriate sequence of coupling of angular momenta by exploiting the invariances of our Hamiltonian. In this way, we can decompose the system of equations into independent parts. In the two- and three-nucleon-systems considered we can assume

- rotational invariance,
- invariance of parity by reflection in space,
- invariance of parity by reflection in isospin space in case of charge independent potentials
- time reversal invariance.

Using these symmetries we get the following conservations:

- in *two-body systems*
  - S Magnitude of total spin
  - $\vec{J}$ Total angular momentum
  - π Parity (reflection in space)

  - $\vec{T}$ Total isospin

- in *three-body systems*
  - $\vec{\Gamma}$ Total angular momentum
  - Π Parity
- in addition: by charge-independent potentials
  - $\vec{T}$ Total isospin

We will use in the following the so-called channel spin representation, i.e., a sequence of couplings with primary coupling of the angular momenta in the subsystems. With this choice, we can use the conservation laws for the two-body systems also in three-body systems.
One has to couple the spins of the nucleons, the angular momenta of $\vec{p}$ and $\vec{q}$, and the corresponding isospins, because we handle neutron and proton as indistinguishable. We will manage the coupling of different angular momenta according to the schema given below:

- ***two-body system*** (β)

  The total spin $\vec{S}_\beta$ is composed of the single spins $\vec{s}_\alpha$ and $\vec{s}_\gamma$. The total angular momentum $\vec{J}_\beta$ results from coupling the angular momentum $\vec{L}_\beta$ with the total spin $\vec{S}_\beta$. The total isospin $\vec{T}_\beta$ is composed of the two single isospins $\vec{\tau}_\alpha$ and $\vec{\tau}_\gamma$. The coupling order is described below:

$$\left.\begin{array}{r}\text{orbital angular momentum } \vec{L}_\beta \\ \left.\begin{array}{r}\vec{s}_\alpha \\ \vec{s}_\gamma\end{array}\right\} \text{subsystem spin } \vec{S}_\beta\end{array}\right\} \text{total angular momentum } \vec{J}_\beta$$

$$\left.\begin{array}{r}\vec{\tau}_\alpha \\ \vec{\tau}_\gamma\end{array}\right\} \text{subsystem isospin } \vec{T}_\beta$$

  In this subsystem (we will indicate the corresponding equations by "(β)" to point at the chosen system of coordinates), one can define a basis

$$\langle(\beta)p(LS)JM_J;TM_T|\,, \tag{2.43}$$

  where the statement of orthogonality is

$$\langle(\beta)p(LS)JM_J;TM_T|p'(L'S')J'M'_J;T'M'_T(\beta)\rangle \tag{2.44}$$
$$= \frac{\delta(p-p')}{p^2}\delta_{SS'}\delta_{LL'}\delta_{JJ'}\delta_{M_JM'_J}\delta_{TT'}\delta_{M_TM'_T} \tag{2.45}$$

and

$$1_\beta = \sum_{LSJT} \sum_{M_T M_J} \int_0^\infty dp\, p^2 |p(LS)JM_J;TM_T(\beta)\rangle\langle(\beta)p(LS)JM_J;TM_T| \,. \tag{2.46}$$

- ***three-body system***

  There, the channel spin $\vec{k}_\beta$ is composed of the total angular momentum of the subsystem β, i.e., $\vec{J}_\beta$ as introduced above, and the single spin $\vec{s}_\beta$ of the third free particle. The total angular momentum $\vec{\Gamma}$ results from the relative angular momentum $\vec{l}_\beta$ and the channel spin $\vec{k}_\beta$. The total isospin of the subsystem $\vec{T}_\beta$ and the isospin of the free particle $\vec{\tau}_\beta$ make up the total isospin of the three-body system. The order of coupling is outlined below:

$$\left.\begin{array}{r}\text{subsystem total-}\\ \text{angular momentum } \vec{J}_\beta\\ \text{single particle spin } \vec{s}_\beta\end{array}\right\} \text{channel spin } \vec{k}_\beta \left.\begin{array}{l}\\ \\ \\ \end{array}\right\} \text{total angular momentum } \vec{\Gamma}$$
$$\text{relative orbital angular momentum } \vec{l}_\beta \;\;\Big\}$$

$$\left.\begin{array}{r}\text{subsystem isospin } \vec{T}_\beta\\ \text{free particle isospin } \vec{\tau}_\beta\end{array}\right\} \text{total isospin } \vec{I}$$

  We can introduce the states of a three-body system as

$$|pq(((LS)Js)kl)\Gamma M_\Gamma;(T\tau)IM_I(\beta)\rangle \,, \tag{2.47}$$

  with the normalization

$$\begin{aligned}&\langle(\beta)pq(((LS)Js)kl)\Gamma M_\Gamma;(T\tau)IM_I|p'q'(((L'S')J's')k'l')\Gamma' M'_\Gamma;(T'\tau')I'M'_I(\beta)\rangle\\ &= \frac{\delta(p-p')}{p^2}\frac{\delta(q-q')}{q^2}\delta_{LL'}\delta_{SS'}\delta_{JJ'}\delta_{ss'}\delta_{kk'}\delta_{ll'}\delta_{\Gamma\Gamma'}\delta_{M_\Gamma M'_\Gamma}\delta_{TT'}\delta_{\tau\tau'}\delta_{II'}\delta_{M_I M'_I}\end{aligned} \tag{2.48}$$

  and

$$\begin{aligned}1_\beta = \sum_{LSJs}\sum_{kl\Gamma\tau}\sum_{TIM_TM_J}\int_0^\infty dp\, p^2 \; &|pq(((LS)Js)kl)\Gamma M_\Gamma;(T\tau)IM_I\rangle\\ &\langle pq(((LS)Js)kl)\Gamma M_\Gamma;(T\tau)IM_I| \,.\end{aligned} \tag{2.49}$$

After decomposing the angular momentum in our three-body system, we go over to the partial wave decomposition of three-body states

$$\langle(\beta)\,\underbrace{\vec{q}sm_s\,\tau m_\tau}_{\text{relative}};\underbrace{\vec{p}SM_S TM_T}_{\text{subsystem}}| \,, \tag{2.50}$$

using the invariances mentioned above, and the denoted order of coupling and obtain

$$\langle \vec{p}| = \sum_{LM_L} \langle pLM_L|Y_{LM_L}(\hat{p})\,. \tag{2.51}$$

If we take into account spin and isospin, $\langle \vec{p}|$ is given as

$$\langle \vec{p}|\langle SM_S|\langle TM_T| = \sum_{JM_J}\sum_{LM_L} \langle p(LS)JM_J;TM_T| \left(\begin{array}{cc|c} L & S & J \\ M_L & M_S & M_J \end{array}\right) Y_{LM_L}(\hat{p})\,, \tag{2.52}$$

and with the two-body state

$$\langle \vec{q}|\langle sm_s|\langle \tau m_\tau| = \sum_{lm_l} \langle qsm_s;\tau m_\tau|Y_{lm_l}(\hat{q}) \tag{2.53}$$

we obtain for the basis (2.50)

$$\begin{aligned}\langle (\beta)\vec{q}sm_s\,\tau m_\tau;\vec{p}SM_STM_T| &= \sum_{LM_L}\sum_{JM_J}\sum_{km_k}\sum_{lm_l}\sum_{\Gamma M_\Gamma}\sum_{IM_I} Y_{LM_L}(\hat{p})\,Y_{lm_l}(\hat{q}) \\ &\times \left(\begin{array}{cc|c} L & S & J \\ M_L & M_S & M_J \end{array}\right)\left(\begin{array}{cc|c} J & s & k \\ M_J & m_s & m_k \end{array}\right)\left(\begin{array}{cc|c} k & l & \Gamma \\ m_k & m_l & M_\Gamma \end{array}\right) \\ &\times \left(\begin{array}{cc|c} T & \tau & I \\ M_T & m_\tau & M_I \end{array}\right) \langle (\beta)pq(((LS)Js)kl)\Gamma M_\Gamma;(T\tau)IM_I|\,. \end{aligned} \tag{2.54}$$

For numerical calculation, we have to restrict some of the quantum numbers, because of the infinite number of states in (2.54). Therefore, we use some of the conservation laws, like conservation of total angular momentum given as a coupling of total angular momentum of triton to the incoming photon (for photodisintegration). Besides, the subsystem total angular momentum is restricted to $J \leq 1^+$, $J \leq 1^+$, $J \leq 2^+$ and $J \leq 2$ in different calculations, as will be discussed in Section 5.9.

2.4.1 Decomposition of the channel states

Now, we can use the described decomposition of angular momentum to expand the channel states $\langle \Phi_\beta|$ in three-body basis states (2.50). A channel state is a tensor product of a plane wave $\langle (\beta)\vec{q}sm_s;\tau m_\tau|$ and a bound state wave function $\langle (\beta)\Psi^{(SJ^\pi;T)}M_JM_T|$ where

$$\langle \Phi_\beta| = \langle (\beta)\vec{q}\,sm_s;\tau m_\tau| \otimes \langle (\beta)\Psi^{(SJ^\pi;T)}M_JM_T|\,. \tag{2.55}$$

Inserting a two-body completeness (2.46) yields

$$\langle\Phi_\beta| = \sum_L \int_0^\infty dp\, p^2 \langle(\beta)\Psi^{(SJ^\pi;T)} M_J M_T | p(LS)JM_J; TM_T(\beta)\rangle \otimes$$
$$\langle(\beta)\vec{q}\, sm_s; \tau m_\tau | \langle(\beta) p(LS)JM_J; TM_T| \,. \tag{2.56}$$

Using the EST-expansion, one can express the bound state wave function under use of angular momentum decomposition as

$$\langle\Psi^{(SJ^\pi;T)}| = \hat{G}_0(E_d) \sum_L \langle gL(SJ^\pi;T)M_J M_T \,| \tag{2.57}$$

and obtain

$$\langle(\beta)\Psi^{(SJ^\pi;T)} M_J M_T | p(LS)JM_J; TM_T(\beta)\rangle = \sum_L G_0(E_d) g_L^{(SJ^\pi;T)}(p)\,. \tag{2.58}$$

Substituting (2.58) into (2.56) and expanding the basis states while taking into account that the subsystem energy is shifted by the energy of the third particle, one can write

$$\begin{aligned}\langle\Phi_\beta| \quad &= \sum_{km_k, lm_l} \sum_{\Gamma M_\Gamma, IM_I} \left(\begin{array}{cc|c} J & s & k \\ M_J & m_s & m_k \end{array}\right) \left(\begin{array}{cc|c} k & l & \Gamma \\ m_k & m_l & M_\Gamma \end{array}\right) \\ &\times \left(\begin{array}{cc|c} T & \tau & I \\ M_T & m_\tau & M_I \end{array}\right) \langle(\beta) gqb\Gamma M_\Gamma; IM_I|\, G_0(E_d + \tfrac{3}{4}q^2 + i0)\,,\end{aligned} \tag{2.59}$$

with the notation

$$\begin{aligned}&\langle(\beta) gqb\Gamma M_\Gamma; IM_I| \\ &= \sum_L \int_0^\infty dp p^2 \langle(\beta) pq(((LS)Js)kl)\Gamma M_\Gamma; (T\tau)IM_I|\; g_L^{(SJ^\pi;T)}(p)\,.\end{aligned} \tag{2.60}$$

One can generalize these so-called partial wave states to rank n, by an index i as

$$\begin{aligned}&\langle(\beta) g_i qb\Gamma M_\Gamma; IM_I| \\ &= \sum_L \int_0^\infty dp p^2 \langle(\beta) pq(((LS)Js)kl)\Gamma M_\Gamma; (T\tau)IM_I|\; g_{Li}^{(SJ^\pi;T)}(p)\,.\end{aligned} \tag{2.61}$$

2.4.2 Integral equation of the transition amplitude

We show here the calculation of the needed transition amplitude by using the partial wave decomposition. We start with the equation (2.33) and multiply this from the right-hand side with $\mathcal{A}H_{em}\,|\Psi_t\rangle$ and from the left-hand side with the partial wave state $\langle(\beta)gqb\Gamma M_\Gamma; IM_I|G_0$

$$\begin{aligned}
&\langle(\beta)gqb\Gamma M_\Gamma; IM_I|\, G_0(E+i0)\Omega^{(-)\dagger}\mathcal{A}H_{em}\,|\Psi_t\rangle \\
&\quad = \langle(\beta)gqb\Gamma M_\Gamma; IM_I|G_0(E+i0)\mathcal{A}H_{em}\,|\Psi_t\rangle \\
&\quad + \sum_\beta \bar{\delta}_{\beta\gamma}\langle(\beta)gqb\Gamma M_\Gamma; IM_I|G_0(E+i0)\,T_\beta(E+i0)\,G_0(E+i0)\,\Omega^{(-)\dagger}\,\mathcal{A}H_{em}\,|\Psi_t\rangle\,,
\end{aligned} \tag{2.62}$$

with H_{em} as the Hamiltonian of electromagnetic interaction and $\mathcal{A}$ as the antisymmetrizing operator, as described in Ref. [5,34]. Now, we can use the T-matrix in the EST approximation

$$\hat{T}(E) = \sum_{LL'S}\sum_{JT}\sum_{M_JM_T} |g(LS)JM_J;TM_T\rangle\,\Delta^{(SJ^\pi;T)}(E)\,\langle g(L'S)JM_J;TM_T|\,. \tag{2.63}$$

Inserting the completeness relations (2.46) and (2.49), coupling of the corresponding angular momenta and using the partial wave states (2.60) one obtains

$$\begin{aligned}
&T_\beta(E+i0) = \\
&\quad \sum_{\Gamma M_\Gamma I M_I b}\int_0^\infty dq\,q^2|gqb\Gamma M_\Gamma; IM_I\,(\beta)\rangle\,\hat{\Delta}^{(SJ^\pi;T)}(E-\frac{3}{4}q^2+i0)\,\langle(\beta)gqb\Gamma M_\Gamma; IM_I|\,.
\end{aligned} \tag{2.64}$$

Inserting (2.64) into (2.62) yields

$$\begin{aligned}
&\langle(\beta)gqb\Gamma M_\Gamma; IM_I|\, G_0(E+i0)\Omega^{(-)\dagger}\mathcal{A}H_{em}\,|\Psi_t\rangle \\
&\quad = \langle(\beta)gqb\Gamma M_\Gamma; IM_I|\, G_0(E+i0)\mathcal{A}H_{em}\,|\Psi_t\rangle \\
&\quad + \sum_\gamma \bar{\delta}_{\beta\gamma}\sum_{\Gamma' M'_\Gamma; I' M'_I b'}\int_0^\infty dq'\,q'^{\,2}\langle(\beta)gqb\Gamma M_\Gamma; IM_I|\, G_0(E+i0)|g'q'b'\Gamma' M'_\Gamma; I'M'_I\,(\gamma)\rangle \\
&\quad \times \hat{\Delta}^{(SJ^\pi;T)'}(E-\frac{3}{4}q^2+i0)\,\langle(\gamma)g'q'b'\Gamma' M'_\Gamma; I'M'_I|\, G_0(E+i0)\Omega^{(-)\dagger}\mathcal{A}H_{em}\,|\Psi_t\rangle\,.
\end{aligned} \tag{2.65}$$

For abbreviation we introduce

$${}^{\Gamma I}\mathcal{AB}^b(q,E) = \langle(\beta)gqb\Gamma; I|\, G_0(E+i0)\,H_{em}\,|\mathcal{A}\Psi_t\rangle\,, \tag{2.66}$$

$$ {}^{\Gamma I}\mathcal{AM}^b(q,E) = \langle(\beta)gqb\Gamma;I|\, G_0(E+i0)\,\Omega^{(-)\dagger}\mathcal{A}H_{em}\,|\mathcal{A}\Psi_t\rangle \tag{2.67} $$

and the effective potential

$$ {}^{\Gamma I}\mathcal{AV}^{bb'}(q,E) = \sum_\beta \bar{\delta}_{\beta\gamma}\langle(\beta)gqb\Gamma;I|\, G_0(E+i0)|g'q'b'\Gamma;I(\gamma)\rangle\,. \tag{2.68} $$

The expression (2.68) is diagonal in Γ and I due to the conservation of the total orbital angular momentum and isospin. Therefore, the effective potential is independent of M_Γ and M_I. Because of the antisymmetrizing operator and the resulting summation over the clusters, ${}^{\Gamma I}\mathcal{AB}^b$ and ${}^{\Gamma I}\mathcal{AM}^b$ are independent of the clustering, so that one does not need to indicate the equations by (β). Detailed investigations on antisymmetrizing are done in Ref. [5,34]. For an effective potential we can write as well that

$$ \langle(\beta)gqb\Gamma;I|\, G_0(E+i0)\,|g'q'b'\Gamma;I(\gamma)\rangle = \langle(\beta)gqb\Gamma;I|\, G_0(E+i0)\,|g'q'b'\Gamma;I(\alpha)\rangle \tag{2.69} $$

and obtain

$$ {}^{\Gamma I}\mathcal{AV}^{bb'}(q,q',E+i0) = 2\langle(\beta)gqb\Gamma M_\Gamma;IM_I|\, G_0(E+i0)\,|g'q'b'\Gamma M_\Gamma;IM_I(\gamma)\rangle\,. \tag{2.70} $$

Now, expression (2.65) has the following form

$$ \begin{aligned} {}^{\Gamma I}\mathcal{AM}^b(q,E_d+\frac{3}{4}q^2) &= {}^{\Gamma I}\mathcal{AB}^b(q,E_d+\frac{3}{4}q^2) \\ &+ \sum_{b'}\int_0^\infty dq'\,q'^{\,2}\,{}^{\Gamma I}\mathcal{AV}^{bb'}(q,q',E_d+\frac{3}{4}q^2) \\ &\times \hat{\Delta}^{(SJ^\pi;T)'}(E_d+\frac{3}{4}q^2-\frac{3}{4}q'^{\,2})\,{}^{\Gamma I}\mathcal{AM}^{b'}(q',E_d+\frac{3}{4}q^2)\,. \end{aligned} \tag{2.71} $$

As in the case of (2.61), one can express (2.71) in the case of an interaction of rank n through the components

$$ \begin{aligned} {}^{\Gamma I}\mathcal{AM}^b_i(q,E_d+\frac{3}{4}q^2) &= {}^{\Gamma I}\mathcal{AB}^b_i(q,E_d+\frac{3}{4}q^2) \\ &+ \sum_{jk}\sum_{b'}\int_0^\infty dq'\,q'^{\,2}\,{}^{\Gamma I}\mathcal{AV}^{bb'}_{ij}(q,q',E_d+\frac{3}{4}q^2) \\ &\times \hat{\Delta}^{(SJ^\pi;T)'}_{jk}(E_d+\frac{3}{4}q^2-\frac{3}{4}q'^{\,2})\,{}^{\Gamma I}\mathcal{AM}^{b'}_k(q',E_d+\frac{3}{4}q^2)\,. \end{aligned} \tag{2.72} $$

With the off-shell extension – i.e., terms which do not fulfill the energy conservation – one obtains the following integral equation system:

$$ \begin{aligned} {}^{\Gamma I}\mathcal{AM}^b(q,E) =& {}^{\Gamma I}\,\mathcal{AB}^b(q,E) \\ &+ \sum_{b'}\int_0^\infty dq'\,q'^{\,2}\,{}^{\Gamma I}\mathcal{AV}^{bb'}(q,q',E)\,\hat{\Delta}^{(SJ^\pi;T)'}(E-\frac{3}{4}q'^{\,2})^{\Gamma I}\mathcal{AM}^{b'}(q',E)\,. \end{aligned} \tag{2.73} $$

This system is numerically solved thankfully by Schadow for three-particle energies from E_d to E_{max}. It should be emphasized that only the on-shell amplitude are observable which are given as

$$\begin{aligned}\langle \mathcal{A}\phi_\beta | \Omega_\beta^{\dagger(-)} T_{em} | \mathcal{A}\Psi_t \rangle &= \sum_{\Gamma=\frac{1}{2}}^{\frac{3}{2}} \sum_{M_\Gamma=-\Gamma}^{\Gamma} \sum_b \sum_{m_k m_l} \left(\begin{array}{cc|c} 1 & \frac{1}{2} & k \\ M_J & M_S & m_k \end{array} \right) \left(\begin{array}{cc|c} k & l & \Gamma \\ m_k & m_l & M_\Gamma \end{array} \right) \\ &\times Y_{lm_l}(\hat{q})\ {}^{\Gamma I}\mathcal{AM}^b(q, E_d + \frac{3}{4}q^2)\,. \end{aligned} \tag{2.74}$$

We will use this latter equation in Section 4 to derive the corresponding amplitude for the capture reaction. For more details we refer to [5], where also the three-body bound states are calculated.

3 Electromagnetic interaction

The interaction between charged particles and the electromagnetic field is well understood in physics [35]. This section will introduce the electromagnetic Hamiltonian with some derivations and applications for photodisintegration and also the capture reaction.

3.1 Basics

The interaction between photons and matter can be described in the first order of approximation with the Coulomb gauge $\vec{\nabla}\vec{A} = 0$ as

$$H_{em} = -\int d^3x\, \vec{j}(\vec{x})\vec{A}(\vec{x}) \tag{3.1}$$

in terms of a nuclear current operator $\vec{j}(\vec{x})$ and the electromagnetic potential operator $\vec{A}(\vec{x})$ (note: $\hbar = c = 1$). As usual, the current has to obey the continuity equation

$$-\vec{\nabla}\vec{j} = \dot{\rho} = [H_N, \rho(\vec{x})] \tag{3.2}$$

to ensure charge conservation. H_N represents the nuclear Hamiltonian, which describes the concerned nucleons as well as the particle exchange current. The current and charge density are composed of single- and many-particle terms:

$$\rho = \rho_{[1]} + \rho_{[2]} + \cdots \qquad \vec{j} = \vec{j}_{[1]} + \vec{j}_{[2]} + \cdots . \tag{3.3}$$

The single-particle operators

$$\rho_{[1]} = \sum_i \rho_i \qquad \text{and} \qquad \vec{j}_{[1]} = \sum_i \vec{j}_i \tag{3.4}$$

describe the nucleons, while the many-particle operators go on the currents of the exchange particles, i.e. the interaction between the particles.

3.2 Siegert's hypothesis

For an adequate description of nuclear precesses one has to take into account many-particle currents, which are commonly unknown. With Siegert's hypothesis [36] it is possible to consider them even with no detailed knowledge. One can do this operation by expanding the continuity equation in terms of single and many particles:

$$\begin{aligned} 0 = \vec{\nabla}\cdot\vec{j} + i[H_N, \rho] &= \vec{\nabla}\cdot\vec{j}_{[1]} + i[T, \rho_{[1]}] \\ &+ \vec{\nabla}\cdot\vec{j}_{[2]} + i[T, \rho_{[2]}] + i[V_{[2]}, \rho_{[1]}] \\ &+ \cdots . \end{aligned} \tag{3.5}$$

Separating (3.5) into single- and many-particle operators yields

$$0 = \vec{\nabla} \cdot \vec{j}_{[1]} + i[T, \rho_{[1]}] \tag{3.6}$$
$$0 = \vec{\nabla} \cdot \vec{j}_{[2]} + i[T, \rho_{[2]}] + i[V_{[2]}, \rho_{[1]}] \, . \tag{3.7}$$

The single-particle operator does not fulfill (3.2) without fail. If the potential depends on isospin or momentum (this is the case for realistic potentials), then the commutator $[T, \rho_{[2]}]$ does not vanish so that $\vec{\nabla} \cdot \vec{j}_{[2]} \neq 0$.

The hypothesis of Siegert implies that in a nonrelativistic approximation the charge density of the exchange particles and thus their contributions to the two-particle charge density in (3.7) vanish.

One can then write

$$\rho = \rho_{[1]} \tag{3.8}$$

and for the continuity equation

$$(\vec{\nabla} \cdot \vec{j} = \vec{\nabla} \cdot \vec{j}_{[1]} + \vec{\nabla} \cdot \vec{j}_{[2]}) = -\dot{\rho}_{[1]} \, . \tag{3.9}$$

This means, that $\dot{\rho}_{[1]}$ contains parts of the exchange currents already. They are the longitudinal parts, because of the chosen gauge above and the resulting continuity equation (3.2). We will use only these longitudinal currents in the following calculations.

3.3 Siegert's theorem

Now, one can introduce an equation for the transversal components. Transforming the continuity equation (3.2) into momentum space with

$$\tilde{\vec{j}}(\vec{k}_\gamma) = \int d^3x \vec{j}(\vec{x}) \, e^{i\vec{k}_\gamma \vec{x}} \tag{3.10}$$

and the charge density

$$\tilde{\rho}(\vec{k}_\gamma) = \int d^3x \rho(\vec{x}) \, e^{i\vec{k}_\gamma \vec{x}} \tag{3.11}$$

provides

$$\vec{k}_\gamma \cdot \tilde{\vec{j}}(\vec{k}_\gamma) = -i \, \dot{\tilde{\rho}}(\vec{k}_\gamma) = [H_N, \tilde{\rho}(\vec{k}_\gamma)] \, . \tag{3.12}$$

The latter equation (3.12) depicts the longitudinal components of the current. Building the gradient of both sides of (3.12) with $\vec{k}_\gamma = 0$ (low energy approximation) enables us to

derive the transversal components and leads to the original form of Siegert's theorem:

$$\tilde{\vec{j}}(0) = [\, H_N, \underbrace{\int d^3x \rho(\vec{x})\, \vec{x}}_{\vec{D}} \,]\,. \tag{3.13}$$

According to Siegert's theorem this approximation (i.e. the commutator between H_N and the dipole operator $\vec{D}$) is pertinent, because the two-particle current densities are well described due to the gauge condition. It should be stressed again that this theorem is valid only in $\vec{k}_\gamma \to 0$ limit. This result is obviously useful as it allows to eliminate the technical complications of the current operator (by replacing it with the charge density operator) when evaluating electromagnetic transitions in nuclear calculations.

3.4 Multipole expansion

As mentioned in Section (3.1) the Hamiltonian in the first order of approximation with the Coulomb gauge can be expressed as

$$H_{em} = -\int d^3x\, \vec{j}(\vec{x})\vec{A}(\vec{x})\,. \tag{3.14}$$

By calculation of the cross section the normalization factor of the plane wave will be factored out from H_{em}:

$$H_{em} = \left(\frac{2\pi}{\omega V}\right)^{\frac{1}{2}} T_{em}(\vec{k}_\gamma, \lambda) = \left(\frac{2\pi}{\omega V}\right)^{\frac{1}{2}} \int d^3r \hat{\epsilon}_{\vec{k}_\gamma,\lambda} e^{i\vec{k}_\gamma \vec{r}} \vec{j}(\vec{r})\,. \tag{3.15}$$

The photon field $\hat{\epsilon}_{\vec{k}_\gamma,\lambda} e^{i\vec{k}_\gamma \vec{r}}$ can be expanded in electric and magnetic multipoles [37,35]. The direction of the $\vec{z}$- axis is chosen along the momentum of the incoming photon, so that the expansion of T_{em} can be written as

$$T_{em}(\vec{k}_\gamma, \lambda) = -(2\pi)^{\frac{1}{2}} \sum_L \hat{L}[T_{el}^{[L]}(k_\gamma, \lambda) + \lambda T_{mag}^{[L]}(k_\gamma, \lambda)], \qquad \hat{L} = \sqrt{2L+1} \tag{3.16}$$

with $T_{el}^{[L]}$ as electric and $T_{mag}^{[L]}$ as magnetic multipole operators with $(-)^L$ and $(-)^{L+1}$, respectively (L stands for multipolarity). With this separation, one obtains

$$T_{el}^{[L]}(k_\gamma, \lambda) = \frac{i^L}{k_\gamma} \int d^3r [\vec{\nabla} \times j_L(k_\gamma r) \vec{Y}_{LL;\lambda}(\Omega_r)] \cdot \vec{j}(\vec{r}) \tag{3.17}$$

$$T_{mag}^{[L]}(k_\gamma, \lambda) = i^L \int d^3r [j_L(k_\gamma r) \vec{Y}_{LL;\lambda}(\Omega_r)] \cdot \vec{j}(\vec{r})\,. \tag{3.18}$$

The expressions in the squared parenthesis are substantially the multipoles of the electromagnetic vector potential $\vec{A}$ and give rise, in the long-wave-length limit, to the

electric and the magnetic field, respectively. Furthermore, $j_L(k_\gamma r)$ are the spherical Bessel functions and $\vec{Y}_{LL;\lambda}(\Omega_r)$ are vector spherical harmonics.

The transition amplitude $T_{em}(\vec{k}_\gamma, \lambda)$ is, therefore, the coherent superposition of the electric and magnetic matrix elements, which are compatible with the general conservation principles. If the states $|i\rangle$ and $|f\rangle$ have a definite spin J_i and J_f, then due to the parity conservation, one can write

$$\begin{aligned} \langle J_f|T^{[L]}_{el}(k_\gamma,\lambda)|J_i\rangle &= (-)^{\pi_f+L+\pi_i}\langle J_f|T^{[L]}_{el}(k_\gamma,\lambda)|J_i\rangle \qquad (3.19)\\ \langle J_f|T^{[L]}_{mag}(k_\gamma,\lambda)|J_i\rangle &= (-)^{\pi_f+L+1+\pi_i}\langle J_f|T^{[L]}_{mag}(k_\gamma,\lambda)|J_i\rangle\,, \qquad (3.20) \end{aligned}$$

where π_i and π_f are the parities of initial and final states ,$|i\rangle$ and $|f\rangle$ respectively.

Now, the electric multipole operator (3.17) can be split in two parts

$$T^{[L]}_{el}(k_\gamma,\lambda) = T^{[L]}_a(k_\gamma,\lambda) + T^{[L]}_b(k_\gamma,\lambda)\,, \qquad (3.21)$$

with

$$\begin{aligned} T^{[L]}_a(k_\gamma,\lambda) &= \frac{i^{L+1}}{k_\gamma}\frac{1}{\sqrt{L(L+1)}}\int d^3r\,(\vec{\nabla}\Phi_{L\lambda})\cdot\vec{j}(\vec{r})\,,\\ T^{[L]}_b(k_\gamma,\lambda) &= i^{L+1}\frac{1}{\sqrt{L(L+1)}}\int d^3r\,[\vec{r}\,j_L(k_\gamma,\lambda)Y_{L\lambda}(\Omega_r)]\cdot\vec{j}(\vec{r})\,, \end{aligned} \qquad (3.22)$$

and

$$\Phi_{L\lambda} = \left(1 + r\frac{d}{dr}\right) j_L(k_\gamma,\lambda)Y_{L\lambda}(\Omega_r)\,. \qquad (3.23)$$

Integrating by parts, the multipole operator $T^{[L]}_a(k_\gamma,\lambda)$ becomes

$$T^{[L]}_a(k_\gamma,\lambda) = -\frac{i^{L+1}}{k_\gamma}\frac{1}{\sqrt{L(L+1)}}\int d^3r\;\Phi_{L\lambda}\underbrace{[\vec{\nabla}\cdot\vec{j}(\vec{r})]}_{=-[H_N,\rho(r)]}\,. \qquad (3.24)$$

With the replacement above (according to continuity equation (3.2)), we can write for this part of the electric multipole operator

$$T^{[L]}_a(k_\gamma,\lambda) = [H_N\,,\,D_L] \qquad (3.25)$$

and with $H = T + V$

$$T^{[L]}_a(k_\gamma,\lambda) = [T\,,\,D_L] + [V\,,\,D_L]\,, \qquad (3.26)$$

where

$$D_L(k_\gamma,\lambda) = -\frac{i^L}{k_\gamma}\frac{1}{\sqrt{L(L+1)}}\int d^3r\,\rho(r)\left(1+r\frac{d}{dr}\right)j_L(k_\gamma,\lambda)Y_{L\lambda}(\Omega_r)\,. \tag{3.27}$$

In the long-wave-length limit, the $T_a^{[L]}$ part dominates:

$$T_{el}^{[L]} \rightsquigarrow T_a^{[L]} \tag{3.28}$$

The electric transition amplitude is, therefore, only a function of the chare density operator (according to Siegert's theorem). One can replace the Bessel functions by an expansion in small arguments (i.e. $k \to 0$) and express the operator D_L as

$$D_L = i^L\sqrt{\frac{L+1}{L}}\frac{k_\gamma^{L-1}}{(2L+1)!!}\int d^3r\,r^L\rho(\vec{r})Y_{L\lambda}(\Omega_r)\,. \tag{3.29}$$

Assuming a localized charge distribution

$$\rho(\vec{r}) = \sum_{i=1}^{N} e_i\delta(\vec{r}-\vec{r}')\,, \tag{3.30}$$

i.e. for pointlike nucleons, D_L is

$$\begin{aligned} D_L &= i^L\sqrt{\frac{L+1}{L}}\frac{k_\gamma^{L-1}}{(2L+1)!!}\sum_{i=1}^{N} e_i r_i^L Y_{L\lambda}(\Omega_r) \\ &= i^L\sqrt{\frac{L+1}{L}}\frac{k_\gamma^{L-1}}{(2L+1)!!}\sum_{i=1}^{N} e_i\,\mathcal{Y}_{L\lambda}(\vec{r}_i)\,, \end{aligned} \tag{3.31}$$

where $\mathcal{Y}_{L\lambda}$ are the spherical harmonics according to [38].

The role of current conservation in the determination of the electric multipoles has also been analyzed by Friar and Fallieros [39]. They give an expression of the general electric multipole, where the Siegert contribution is isolated and the corrections are evaluated at any order in k.

The detailed the matrix elements needed for photodisintegration and radiative capture calculations can be found in Ref. [5]. There is the role of electric dipole and quadrupole transitions shown. We will use these results to calculate the polarization observables and interprete the achieved outcomes in Section 5.

4 Polarization

This section treats the general formalism of polarization calculations and in particular calculations of vector and tensor analyzing power of the radiative capture reaction $p + d \rightarrow {}^3\mathrm{He} + \gamma$, where the colliding particles are of spin $= \frac{1}{2}$ (for proton) and spin $= 1$ (for deuteron). In the following, we apply a notation, where particles with an arrow indicate the particle whose polarization is considered, according to the Madison convention [40].

Such photonuclear or radiative capture reactions are usually calculated by assuming unpolarized incoming and outgoing particles. These treatments yield commonly differential or total cross sections. Then one has to sum over any possible spin states. If the particles are polarized, one can obtain more information about the dynamic of these processes.

A set of measurements which permit to determine all scattering amplitudes of two particles in the initial and final channel is to be called as complete. Simonius has shown in Ref. [41], that for such a complete set it is sufficient to determine the polarization of just two particles.

The concept of calculating polarization observables in a scattering process will be introduced in the following. Since the particles are in general not in a pure state, but in a mixture of states, one uses a density operator – in particular density matrices as their representation in the spin space – to describe such an ensemble of particles.

4.1 Density matrix

If one expresses a general state by $|\lambda\rangle$ and the ensemble of such states by $|\lambda_i\rangle$ with the properties [42]

$$\langle\lambda_i|\lambda_j\rangle = \delta_{ij}\mathbb{1} \qquad \text{and} \qquad \mathbb{1} = \sum_i |\lambda_i\rangle \langle\lambda_i| \,, \tag{4.1}$$

the general density operator for a mixed ensemble is

$$\rho = \sum_i \rho_i |\lambda_i\rangle \langle\lambda_i| \,, \tag{4.2}$$

where $|\lambda_i\rangle \langle\lambda_i|$ is the projection onto the state $|\lambda_i\rangle$, $\sum\limits_i \rho_i = 1$, and

$$\mathrm{Tr}\rho = 1 \,. \tag{4.3}$$

Note that

$$\begin{aligned} \langle A\rangle = \mathrm{Tr}\rho A &= \sum_{i'} \langle\lambda_{i'}|\rho A|\lambda_{i'}\rangle = \sum_{i'i} \rho_i \langle\lambda_{i'}|\lambda_i\rangle \langle\lambda_i|A|\lambda_{i'}\rangle \\ &= \sum_i \rho_i \langle\lambda_i|A|\lambda_i\rangle \,. \end{aligned} \tag{4.4}$$

Since $\langle\lambda_i|A|\lambda_i\rangle$ is the expectation value of A in the state $|\lambda_i\rangle$, one can interpret ρ_i as the probability that the system is in state $|\lambda_i\rangle$. If all but one of the ρ_i are zero, one says that the system is in a *pure state*; otherwise it is in a *mixed state*. One sees from (4.2) that the density operator is obviously hermitian (while ρ_i is real, as needed for probabilities).

The rotation behavior of the density matrix is of high importance, because most of the measurements take place in another frame of reference than the corresponding calculations.

The transition of a state $|sm\rangle$ in spin basis from frame 1 to frame 2 can be expressed as

$$|sm\rangle_2 = \sum_{m'} D^s_{m'm}(\alpha,\beta,\gamma)|sm'\rangle_1 \tag{4.5}$$

where $D^s_{m'm}(\alpha,\beta,\gamma) = D^s_{m'm}$ represents a common unitary rotation matrix with the Euler angles α, β and γ. Further informations about rotation matrices are presented in Appendix A. The states in (4.2) can be expanded in the respective spin states in frame 1 and frame 2 as

$$\begin{aligned} |\lambda_i\rangle &= \sum_m a^i_m |m\rangle_1 \\ &= \sum_{m'} a^i_{m'} |m'\rangle_2 \,. \end{aligned} \tag{4.6}$$

One can relate the coefficients of the expansion as

$$a^i_m = \sum_{m'} D^s_{mm'} b^i_{m'} \,. \tag{4.7}$$

The density operator ρ can now be expressed in terms of its matrix elements $\rho_{\nu\nu'}$ as

$$\begin{aligned} \rho^{(1)}_{\nu\nu'} &= \langle\nu|\rho^{(1)}|\nu'\rangle \\ &= \sum_i \sum_{mm'} \rho_i a^i_m a^{i^*}_{m'} \langle\nu|m\rangle\langle m'|\nu'\rangle \\ &= \sum_i \rho_i \, a^i_\nu a^{i^*}_{\nu'} \,, \end{aligned} \tag{4.8}$$

so that one can write the transition of the density matrix between the two frames as

$$\rho^{(1)}_{\nu\nu'} = \sum_{\mu\mu'} D^s_{\nu\mu} \rho^{(2)}_{\mu\mu'} \, D^{s^*}_{\nu'\mu'} \,, \tag{4.9}$$

or

$$\rho^{(1)} = D^s \, \rho^{(2)} \, D^{s^\dagger} \,. \tag{4.10}$$

The unitarity of the rotation matrix yields

$$\rho^{(2)} = D^{s\dagger}\,\rho^{(1)}\,D^{s}\,. \tag{4.11}$$

The density matrix of particles with spin s can be expanded in a basis of $(2s+1)^2$ linearly independent matrices. ***The coefficients of expansion are then the polarization of the ensemble, i.e. they are the expectation values of the tensor operators.*** As representation of such a basis, one takes the matrix-representation of spherical or Cartesian tensor operators.

Now, we describe the basis and the resulting density operators of ensembles with $s = \frac{1}{2}$ or $s = 1$ particles, before we go over to ensembles composed of $s = \frac{1}{2}$ and $s = 1$ particles.

4.1.1 Spin-$\frac{1}{2}$ particles

The (2×2)-Pauli matrices

$$\sigma_1 = \begin{pmatrix} 0 & 1 \\ 1 & 0 \end{pmatrix}, \qquad \sigma_2 = \begin{pmatrix} 0 & -i \\ i & 0 \end{pmatrix}, \qquad \sigma_3 = \begin{pmatrix} 1 & 0 \\ 0 & -1 \end{pmatrix} \tag{4.12}$$

and the identity $\mathbb{1}_2 = \sigma_0$ span the used spin space [43]. In this representation the density matrix is given as

$$\rho(\frac{1}{2}) = \frac{1}{(2s+1)} \sum_{i=0}^{3} p_i \sigma_i = \frac{1}{2}\,\vec{p}\cdot\vec{\sigma}\,. \tag{4.13}$$

To exploit the existing rotational symmetry in our reaction, we introduce a set of spherical matrices

$$\tau_{00} = \mathbb{1}_2\,, \qquad \tau_{10} = \sigma_3\,, \qquad \tau_{1\pm1} = \mp\frac{1}{2}(\sigma_1 \pm i\sigma_2) \tag{4.14}$$

and obtain for the density matrix

$$\rho(\frac{1}{2}) = \frac{1}{2} \sum_{k=0}^{1} \sum_{q=-k}^{+k} t_{k,q}\,\tau^{\dagger}_{k,q}\,. \tag{4.15}$$

4.1.2 Spin-1 particles

As in the spin $= \frac{1}{2}$ case, one introduces the (3×3) Cartesian matrices

$$S_x = \frac{1}{\sqrt{2}} \begin{pmatrix} 0 & 1 & 0 \\ 1 & 0 & 1 \\ 0 & 1 & 0 \end{pmatrix}, \qquad S_y = \frac{i}{\sqrt{2}} \begin{pmatrix} 0 & -1 & 0 \\ 1 & 0 & -1 \\ 0 & 1 & 0 \end{pmatrix}, \qquad S_z = \begin{pmatrix} 1 & 0 & 0 \\ 0 & 0 & 0 \\ 0 & 0 & -1 \end{pmatrix}, \tag{4.16}$$

and tensors of second order, whose components one obtains by symmetrical combination of products of S_i-matrices, taking account of hermiticity and $\mathrm{Tr}(P_{ij}) = 0$. They can be expressed as

$$P_{ij} = \frac{3}{2}(S_i S_j + S_j S_i) - 2\mathbb{1}_3 \,. \tag{4.17}$$

Between these six matrices P_{ij}, one finds the relation

$$P_{11} + P_{22} + P_{33} = 0 \,, \tag{4.18}$$

so that

$$\mathbb{1}_3, S_1, S_2, S_3, P_{12}, P_{13}, P_{23}, P_{33} \text{ and } P_{11-22} (\equiv P_{11} - P_{22}) \tag{4.19}$$

build a linearly independent set of tensors of the second order which span the spin space for spin-1 particles. With this choice the density matrix is to be written as

$$\rho(1) = \frac{1}{3}\left(\mathbb{1}_3 + \frac{3}{2}\sum_{i=1}^{3} p_i \, S_i + \frac{1}{3}\sum_{kl} p_{kl} P_{kl}\right) \,, \tag{4.20}$$

where $(kl) \in \{(12), (13), (23), (33), (11-22)\}$. As in the latter section mentioned, we introduce a set of spherical matrices

$$\begin{aligned} \tau_{00} = \mathbb{1}_3 \,, \qquad & \tau_{10} = \tfrac{\sqrt{3}}{2} S_3 \,, \\ \tau_{1\pm1} = \mp\tfrac{\sqrt{3}}{2}(S_1 \pm i S_2) \,, \qquad & \tau_{2\pm2} = \tfrac{\sqrt{3}}{2}(S_1 \pm i S_2)^2 \end{aligned} \tag{4.21}$$

to exploit the rotational symmetry and obtain for the density matrix

$$\begin{aligned} \rho(1) &= \frac{1}{(2s+1)} \sum_{k=0}^{2} \sum_{q=-k}^{+k} t_{k,q} \, \tau^{\dagger}_{k,q} \\ &= \frac{1}{3} \sum_{k=0}^{2} \sum_{q=-k}^{+k} t_{k,q} \, \tau^{\dagger}_{k,q} \,. \end{aligned} \tag{4.22}$$

4.1.3 Irreducible statistical tensors

An alternative and better representation is offered by the components of the irreducible statistical tensors of rank $k \leq 2s$ [41]. We can introduce them as

$$\langle s\mu' | \tau_{kq} | s\mu \rangle = \hat{s} (-)^{s-\mu} \langle s\mu' \, s - \mu | kq \rangle \,, \tag{4.23}$$

with $\hat{s} = \sqrt{2s+1}$. Here, $\langle s\mu' \, s - \mu | kq \rangle$ is a Clebsch-Gordan coefficient. These tensor elements (4.23) with the property

$$\sum_{kq} \langle s\mu | \tau_{kq} | s\mu' \rangle \, \langle s\nu | \tau^{\dagger}_{kq} | s\nu' \rangle = (2s+1) \delta_{\mu\nu} \, \delta_{\mu'\nu'} \tag{4.24}$$

build a complete basis in the space of complex valued $(2s+1)\times(2s+1)$-matrices. With the orthogonality relation

$$\mathrm{Tr}(\tau_{kq}\,\tau^{\dagger}_{k'q'}) = (2s+1)\delta_{kk'}\delta_{qq'} \tag{4.25}$$

and the coefficients of the expansion

$$\begin{aligned} t_{kq} &= \mathrm{Tr}\,(\rho\,\tau_{kq}) \\ &= \hat{s}\sum_{\mu\mu'}(-)^{s-\mu}\langle s\mu' s-\mu|kq\rangle\,\rho_{\mu\mu'}\,, \end{aligned} \tag{4.26}$$

we can express the density operator ρ as

$$\rho = \frac{1}{2s+1}\sum_{kq} t_{kq}\,\tau^{\dagger}_{kq}\,. \tag{4.27}$$

The components of the density matrix read

$$\rho_{\mu\mu'} = \frac{1}{\hat{s}}\sum_{kq}(-)^{s-\mu}\langle s\mu' s-\mu|kq\rangle\,t_{kq}\,. \tag{4.28}$$

The most important symmetry properties of τ_{kq} can be checked from the corresponding properties of the Clebsch-Gordan coefficients. Note that for all nonzero elements it yields

$$q = \mu' - \mu \tag{4.29}$$

and

$$(\tau_{00})_{\mu'\mu} = \hat{s}(-)^{s-\mu}\langle s\mu' s-\mu|00\rangle = \delta_{\mu\mu'} \tag{4.30}$$

which implies $t_{00} = \mathrm{Tr}(\rho)$ and thus for normalized states

$$t_{00} = 1\,. \tag{4.31}$$

For this normalization we have introduced $\hat{s}$. Furthermore, we can show the hermiticity condition

$$t^{*}_{kq} = (-)^{q}t_{k-q}\,, \tag{4.32}$$

so that all t_{k0} are real valued. The rotational properties of the statistical tensors are given by the corresponding properties (4.9) and (4.10) for density matrices together with the well known Clebsch-Gordan decomposition of products of rotation matrices and

$$D^{s}_{mm'} = (-)^{(m-m')}\,D^{s*}_{-m-m'}\,. \tag{4.33}$$

The property (4.33) is the reason for introducing the phase $(-)^{s-\mu}$ in (4.23). We then obtain for the transformation from frame 1 to frame 2

$$t_{kq}^{(1)} = \sum_{q'} D_{qq'}^{s,k^*} \; t_{kq'}^{(2)} \,. \tag{4.34}$$

Here only one single rotation matrix appears, which is in contrary to the transformation relation of the density matrix (4.9).

We now show the relationship between the components of t_{kq} and the expansion coefficients $\vec{p}$ occurring in (4.13) or (4.20), respectively:

- spin-$\frac{1}{2}$ particles:

$$\begin{aligned} t_{10} &= p_3 \\ t_{1\pm1} &= \mp\frac{1}{\sqrt{2}}(p_3 \pm i p_2) \end{aligned} \tag{4.35}$$

- spin-1 particles:

$$\begin{aligned} t_{10} &= \sqrt{\frac{3}{2}}\, p_3 \\ t_{1\pm1} &= \mp\frac{\sqrt{3}}{2}(p_1 \pm i p_2) \\ t_{20} &= \frac{1}{\sqrt{2}} p_{33} \\ t_{2\pm1} &= \mp\frac{1}{\sqrt{3}}(p_{13} \pm i p_{23}) \\ t_{2\pm2} &= \frac{1}{2\sqrt{3}}(p_{11} - p_{22} \pm i p_{12}) \end{aligned} \tag{4.36}$$

For higher spins, one needs higher tensors which, in order to be irreducible, again must be symmetric and traceless for any pair of indices. The great advantage of using these components of statistical tensors concerning the computational efforts, should also be emphasized here. This choice fulfills the Madison convention as well. In the following, we will use only this set.

4.1.4 Composite systems

For a composed system of protons and deuterons we have to build a total density operator as

$$\rho = \rho(\frac{1}{2}) \otimes \rho(1) \,. \tag{4.37}$$

Using the notation

$$Z_{k_p q_p, k_d q_d} = \tau^{(\frac{1}{2})\dagger}_{k_p q_p} \otimes \tau^{(1)\dagger}_{k_d q_d} \qquad \text{and} \qquad z_{k_p q_p, k_d q_d} = t^{(\frac{1}{2})}_{k_p q_p}\, t^{(1)}_{k_d q_d} \tag{4.38}$$

one can write

$$\rho = \frac{1}{6} \sum_{k_p=0}^{1} \sum_{q_p=-k_p}^{+k_p} \sum_{k_d=0}^{2} \sum_{q_d=-k_d}^{+k_d} z_{k_p q_p, k_d q_d}\; Z_{k_p q_p, k_d q_d}\,, \tag{4.39}$$

and obtains again

$$z_{k_p q_p, k_d q_d} = \mathrm{Tr}(\rho\, Z_{k_p q_p, k_d q_d})\,. \tag{4.40}$$

Now, we can use this derived density operator to describe the phenomena and observables of photonuclear reactions.

4.2 Transition matrix for the photodisintegration

As discussed in Ref. [5], we convert the T-matrix into a form we need for polarization calculations. One can write

$$M = C \cdot \langle \phi_\alpha | \Omega^{\dagger\,(-)} \mathcal{A}\, T_{em} \,|\Psi_t\,\rangle\,, \tag{4.41}$$

with

$$C^2 = m_N \hbar \frac{(2\pi)^3}{3\pi c} \frac{q E_\gamma}{4}\,. \tag{4.42}$$

Then we can express M as:

$$\begin{aligned} M &= C \cdot \sum_{\Gamma=\frac{1}{2}}^{\frac{3}{2}} \sum_{M_\Gamma} \sum_{b} \sum_{m_k m_l} \left(\begin{array}{cc|c} J & s & k \\ m_J & m_s & m_k \end{array} \right) \left(\begin{array}{cc|c} k & l & \Gamma \\ m_k & m_l & m_\Gamma \end{array} \right) \\ &\quad \times Y_{l,m_l}(\hat{q})\; {}^{\Gamma l}\mathcal{A}\, \mathcal{M}^b(q, E_d + \frac{3}{4} q^2) \qquad (4.43) \\ &= C \cdot \sum_{m_J=-1}^{+1} \sum_{m_s=-\frac{1}{2}}^{+\frac{1}{2}} \sum_{m_\Gamma=-\frac{1}{2}}^{+\frac{1}{2}} \sum_{M_\lambda=\pm 1} \left(\begin{array}{cc|c} J & s & k \\ m_J & m_s & m_k \end{array} \right) \left(\begin{array}{cc|c} k & l & \Gamma \\ m_k & m_l & m_\Gamma \end{array} \right) \\ &\quad \times (-)^{\Gamma - M_\Gamma} \left(\begin{array}{ccc} \Gamma & \lambda & \Gamma' \\ -M_\Gamma & M_\lambda & M_{\Gamma'} \end{array} \right) Y_{l,m_l}(\hat{q})\, ||^{\Gamma l}\mathcal{A}\, \mathcal{M}^b|| \qquad (4.44) \\ &= M^{m_t M_\lambda}_{m_p M_d} \qquad (4.45) \end{aligned}$$

In the equation (4.44), $||^{\Gamma l}\mathcal{A}\,\mathcal{M}^{b}||$ are the reduced matrix elements of the photodisintegration, which are thankfully delivered by Schadow. In Section 4.3, we will show how to treat the transition matrix of the photodisintegration to obtain the corresponding one for the capture reaction.

From (4.43) to (4.44) we have used that $M_\Gamma = M_\lambda + M_{\Gamma'}$, $m_k = m_s + m_J$, and $m_l = M_\Gamma - m_k$. These identities are given due to the properties of the Clebsch-Gordon coefficients. Furthermore, we can replace three quantum numbers by their fixed values as

$$J = 1\,, \qquad s = \frac{1}{2}\,, \text{ and } \qquad \Gamma' = \frac{1}{2}\,. \tag{4.46}$$

We indicate the quantum numbers $\{sJ^\pi kl, T\tau\}$ by b, as introduced in equation (2.60). The used notation is in according to Lindner [38].

4.3 Rotation

Using available transition amplitudes of photodisintegration to describe the capture process requires some transformation we will discuss in the following. We refer to appendix A for the used rotation matrices and their properties.

4.3.1 Amplitude rotation

First, we have to transform the system of coordinates of the photodisintegration reaction to the coordinates of the capture reaction. One can consider a capture reaction as a time reversed photodisintegration. Note, that for both cases the chosen system is the center-of-mass-system (CMS).

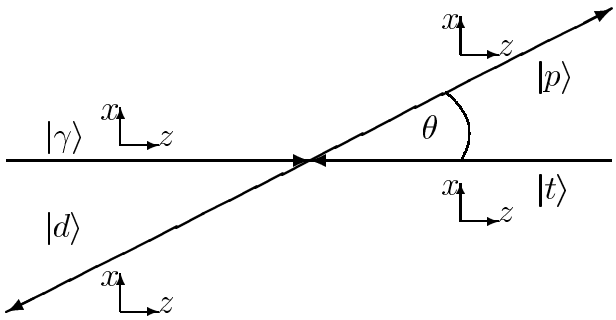

Figure 1: Photodisintegration

Figures 1 and 2 illustrate the reaction with the single coordinates for each participating particle for the photodisintegration and capture, respectively.

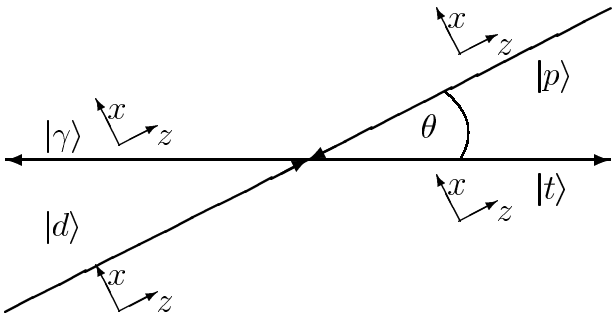

Figure 2: Capture

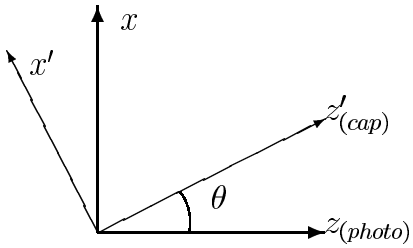

Figure 3: Photo → Capture

For the capture reaction, each of the center-of-mass coordinates have to be turned in a way as sketched in Figure 3.

Note, that in Figure 3 the angle θ is the same as the scattering angle illustrated in the previous Figures 1 or 2. According to the Madison convention [40], the measured angle is always defined between the incoming and the detected outgoing beam.

We can write these rotations as:

$$|m_p\rangle_{cap} = \sum_{m'_p} d^{\frac{1}{2}}_{m'_p m_p}(\theta)|m'_p\rangle_{photo} \tag{4.47}$$

$$|M_d\rangle_{cap} = \sum_{M'_d} d^{1}_{M'_d M_d}(\theta)\,|M'_d\rangle_{photo} \tag{4.48}$$

$${}_{cap}\langle m_t| = \sum_{m'_t} d^{\frac{1}{2}}_{m'_t m_t}(\theta)\,{}_{photo}\langle m'_t| \tag{4.49}$$

$${}_{cap}\langle M_\lambda| = \sum_{M'_\lambda} d^{1}_{M'_\lambda M_\lambda}(\theta)\,{}_{photo}\langle M'_\lambda| \tag{4.50}$$

Now, one has to notice, that detailed balance [44] provides for the cross section

$$\frac{d\sigma}{d\Omega}^{cap} = \frac{2\,E_\gamma^2}{3\,q^2}\frac{d\sigma}{d\Omega}^{photo} \quad . \tag{4.51}$$

The general relation for the cross section of the capture reaction is

$$\overline{\frac{d\sigma}{d\Omega}} = \frac{1}{6}\mathrm{Tr}\, M\, M^\dagger \,. \tag{4.52}$$

The factor $\frac{1}{6}$ in (4.52) stems from the averaging the possible spin states. and the fact, that we have to conjugate the transition matrix element $(M^{m_t' M_\lambda'}_{m_p' M_d'})^{photo}$, results in

$$\begin{aligned} {}^{cap}(M^{m_t M_\lambda}_{m_p M_d})(\pi-\theta) &= \sqrt{\frac{2\,E_\gamma^2}{3\,q^2}} \sum_{m_p' M_d'} \sum_{m_t' M_\lambda'} d^{\frac{1}{2}}_{m_p' m_p}(\theta)\, d^1_{M_d' M_d}(\theta) \\ & \quad d^{\frac{1}{2}}_{m_t' m_t}(\theta) d^1_{M_\lambda' M_\lambda}(\theta) (M^{m_p' M_d'}_{m_t' M_\lambda'})^{photo}(\theta) \,. \end{aligned} \tag{4.53}$$

4.3.2 Rotation from CMS into SCM

In this section, we consider the fact that experimental measurements are always in laboratory system. There, the direction of the coordinates correspond to the so called standard center of mass system (SCM), i.e. a right handed center of mass system, whereby the direction of the z-axis is along the momentum of **each** particle and the y-axis along $(\vec{k}_{in} \times \vec{k}_{out})$. This definition is of course in accordance with the Madison convention [40]. The needed system of coordinates and the resulting rotations are illustrated in the following Figures 4 and 5:

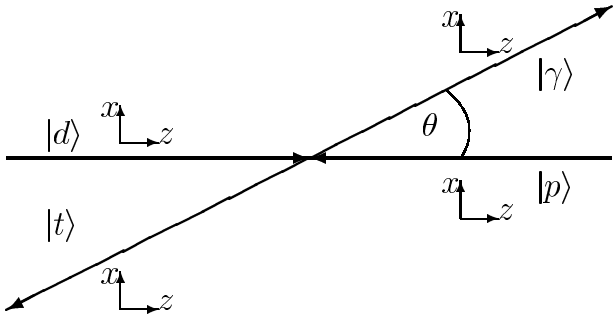

Figure 4: Capture in CMS

One sees that the target coordinates are flipped. We express the sketched rotations from

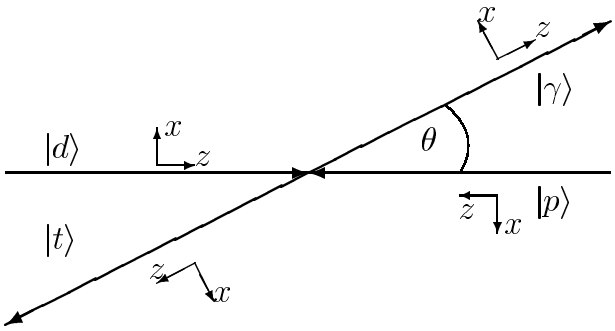

Figure 5: Capture in SCM

Figure 4 into Figure 5 by γ-detecting as

$$\begin{aligned} |m_p\rangle_{SCM} &= \sum_{m'_p} d^{\frac{1}{2}}_{m'_p m_p}(\pi)|m'_p\rangle_{CMS} \\ &= (-)^{\frac{1}{2}-m_p}|-m_p\rangle_{CMS} \qquad (4.54) \\ |M_d\rangle_{SCM} &= |M_d\rangle_{CMS} \qquad (4.55) \end{aligned}$$

$$\begin{aligned} {}_{SCM}\langle m_t| &= \sum_{m'_t} d^{\frac{1}{2}}_{m'_t m_t}(\theta+\pi)\,{}_{CMS}\langle m'_t| \\ &= \sum_{m'_t} (-)^{\frac{1}{2}-m_t}\, d^{\frac{1}{2}}_{m'_t -m_t}(\theta)\,{}_{CMS}\langle m'_t| \qquad (4.56) \\ {}_{SCM}\langle M_\lambda| &= \sum_{M'_\lambda} d^{1}_{M'_\lambda M_\lambda}(\theta)\,{}_{CMS}\langle M'_\lambda| \qquad (4.57) \end{aligned}$$

so that we can combine the results to

$$(M^{m_t M_\lambda}_{m_p M_d})_{SCM} = \sum_{m'_t M'_\lambda} (-)^{1-m_p-m_t}\, d^{\frac{1}{2}}_{m'_t -m_t}(\theta) d^{1}_{M'_\lambda M_\lambda}(\theta)\,(M^{m'_t M'_\lambda}_{-m_p M_d})_{CMS}\,. \qquad (4.58)$$

If triton is detected, one has easily to replace the angle θ by $(\pi+\theta)$ in the equations above.

4.4 Polarization observables

The transformation of the density matrix during the reaction is given as

$$\rho^{out} = M\,\rho^{in}\,M^\dagger\,, \qquad (4.59)$$

where M represents the scattering amplitude. This relationship between the density matrices in the initial and final channel describes also the transformation of the mentioned

basis states, i.e. (4.59) shows the way how the $Z_{k_p q_p, k_d q_d}$ are transformed due to the reaction. Since the transition amplitude M is generally not unitary, ρ^{out} is not traceless. The observables in the final channel can be expressed by

$$\begin{aligned} z_{k_t q_t, k_\lambda q_\lambda} &= \mathrm{Tr}\left(\rho^{out} Z_{k_t q_t, k_\lambda q_\lambda}\right) \\ &= \mathrm{Tr}\left(M\,\rho^{in}\,M^\dagger\, Z_{k_t q_t, k_\lambda q_\lambda}\right) \\ &= \frac{1}{6}\,\mathrm{Tr}\left(M\left[\sum_{k_p q_p}\sum_{k_d q_d} z_{k_p q_p, k_d q_d}\, Z_{k_p q_p, k_d q_d}\right] M^\dagger\, Z_{k_t q_t, k_\lambda q_\lambda}\right) \\ &= \frac{1}{6}\sum_{k_p q_p}\sum_{k_d q_d} z_{k_p q_p, k_d q_d}\,\mathrm{Tr}\, M\, Z_{k_p q_p, k_d q_d}\, M^\dagger\, Z_{k_t q_t, k_\lambda q_\lambda}\,. \end{aligned} \tag{4.60}$$

Now, we can write

$$z_{k_t q_t, k_\lambda q_\lambda} = \sum_{k_p q_p}\sum_{k_d q_d} \frac{\overline{d\sigma}}{d\Omega}\, z_{k_p q_p, k_d q_d}\, T^{k_t q_t, k_\lambda q_\lambda}_{k_p q_p, k_d q_d}\,, \tag{4.61}$$

with

$$T^{k_t q_t, k_\lambda q_\lambda}_{k_p q_p, k_d q_d} = \frac{\mathrm{Tr}\, M\, Z_{k_p q_p, k_d q_d}\, M^\dagger\, Z_{k_t q_t, k_\lambda q_\lambda}}{\mathrm{Tr}\, M\, M^\dagger} \tag{4.62}$$

as the experimental measurable **polarization observables** and

$$\frac{\overline{d\sigma}}{d\Omega} = \frac{1}{6}\,\mathrm{Tr}\, M\, M^\dagger\,, \tag{4.63}$$

for the unpolarized differential cross section of the capture reaction.

The corresponding expression for the polarized differential is now given as

$$\frac{d\sigma}{d\Omega} = \mathrm{Tr}\, M\,\rho M^\dagger\,. \tag{4.64}$$

As shown in Section 4.1.3, there are four different $\tau^{(\frac{1}{2})}_{k_p q_p}$ and nine different $\tau^{(1)}_{k_d q_d}$, so that one obtains 36 possible $Z_{k_p q_p, k_d q_d}$ for each channel, i.e. initial and final channel. It results that there are 36^2 different $T^{k_t q_t, k_\lambda q_\lambda}_{k_p q_p, k_d q_d}$. Using the existing invariances, one can reduce this high number, which we will discuss in the following.

4.5 Symmetry properties

In this section we discuss the application of symmetries to amplitudes and observables. As mentioned, we use the translation and rotation invariances. In the following we will see the impact of parity and time reversal.

4.5.1 Parity symmetry

A free particle state transforms under reflection at the origin according to

$$\Pi\,|\vec{q}_\alpha\rangle = \pi_\alpha|-\vec{q}_\alpha\rangle\,, \tag{4.65}$$

where Π is the parity operator. One sees, that the momentum is reversed. Expressing the state in the spin space, we obtain

$$\Pi\,|\vec{q}_\alpha; M_J m_s\rangle = \pi_\alpha|-\vec{q}_\alpha; M_J m_s\rangle\,, \tag{4.66}$$

thus the spin-state is invariant due to the fact that the rotation operator commutes with the parity operator. π_α is the intrinsic parity of the particle α, and we have assumed that the intrinsic state of α is a pure parity state. It follows that $\pi_\alpha = 1$.
Since the Hamiltonian is parity invariant, it follows for the transition operator Π:

$$\Pi^{-1}\,M\,\Pi = M\,. \tag{4.67}$$

We can describe the reflection above as a rotation of the state in the momentum space about the y-axis by an angle of π, according to the Madison convention:

$$\begin{aligned} D(0,\pi,0)|-\vec{q}; M_J m_s\rangle &= \sum_{M'_J m'_s} |\vec{q}_\alpha; M'_J m'_s\rangle d^{\frac{1}{2}}_{m'_s m_s}(\pi) d^1_{M'_J M_J}(\pi) \\ &= (-)^{1-M_J+\frac{1}{2}-m_s}|\vec{q}_\alpha; -M_J - m_s\rangle\,. \end{aligned} \tag{4.68}$$

Taking into account $D^\dagger\,M\,D = M$, it results

$$\begin{aligned} &\langle\vec{q}'_\alpha; m'_s M'_J|M|\vec{q}_\alpha; M_J m_s\rangle \\ &= \langle\vec{q}'_\alpha; m'_s M'_J|D^\dagger\,M\,D|\vec{q}_\alpha; M_J m_s\rangle \\ &= (-)^{2-M_J-M'_J+1-m_s-m'_s}\langle\vec{q}'_\alpha; -m'_s - M'_J|M|\vec{q}_\alpha; -M_J - m_s\rangle\,, \end{aligned} \tag{4.69}$$

And one obtains for the transition matrix (4.45)

$$M^{m'_s M'_J}_{m_s M_J} = (-)^{2-(M_J+M'_J)}(-)^{1-(m_s+m'_s)}M^{-m'_s-M'_J}_{-m_s-M_J}\,. \tag{4.70}$$

Note that the latter expression is independent of the chosen system of coordinates [45]. The used rotation matrices are described in appendix A.

4.5.2 Time reversal invariance

Time reversal means, practically seen, the exchange of initial and final states [43]. Assuming T as the respective operator, one obtains

$$T^\dagger \vec{p} T = -\vec{p} \qquad \text{and} \qquad T^\dagger \vec{s} T = -\vec{s} \tag{4.71}$$

and therefore

$$T|\vec{q}_\alpha; M_J m_s\rangle = (-)^{1-M_J+\frac{1}{2}-s_s} \,|-\vec{q}_\alpha; -M_J - m_s\rangle\,. \tag{4.72}$$

Because of the antilinearity of T, on can write

$$T^\dagger\, M\, T = M^\dagger\,. \tag{4.73}$$

The direction of the y-axis is turned into the opposite direction by the time reversal transformation. To apply the Madison convention, one has to rotate all systems about the z-axis by an angle of π:

$$D(\pi,0,0)|j,m_j\rangle = e^{im_j\pi}\,|j,m_j\rangle\,. \tag{4.74}$$

With this, we can express the symmetry property due to time reversal as

$$M^{m_s' M_J'}_{m_s M_J} = (-)^{M_J'-M_J+m_s'-m_s}\, M^{m_s M_J}_{m_s' M_J'}\,. \tag{4.75}$$

4.5.3 Properties of the polarization observables

In analogy to (4.32), we can write for the polarization observables of the capture reaction $p+d \to t+\lambda$:

- **Hermiticity**

$$\left(T^{k_t q_t, k_\lambda q_\lambda}_{k_p q_p, k_d q_d}\right)^* = (-)^{k_p+k_d+k_t+k_\lambda}\, T^{k_t q_t, k_\lambda q_\lambda}_{k_p q_p, k_d q_d} \tag{4.76}$$

- **Parity invariance**

$$T^{k_t q_t, k_\lambda q_\lambda}_{k_p q_p, k_d q_d} = (-)^{k_p+q_p+k_d+q_d+k_t+q_t+k_\lambda+q_\lambda}\, T^{k_t -q_t, k_\lambda -q_\lambda}_{k_p -q_p, k_d -q_d} \tag{4.77}$$

- **Time reversal invariance**

$$T^{k_t q_t, k_\lambda q_\lambda}_{k_p q_p, k_d q_d} = (-)^{q_p+q_d+q_t+q_\lambda} T^{k_p q_p, k_d q_d}_{k_t q_t, k_\lambda q_\lambda} \tag{4.78}$$

In (4.76) one sees that for an even phase all polarization observables are real but otherwise always imaginary.

These relationships reduce the number of possible observables discussed in Section 4.4. We can classify the observables using these properties and obtain only 25 independent observables. Note that (4.78) is only valid in the standard-center-of-mass system introduced in Section 4.3.2.
z

4.6 Reduction of the number of polarization observables

First, we show the method of the construction of all possible observables. In the following, we will use the collective quantum number η for all incoming and η' for all outgoing particles in the expression (4.62).

4.6.1 All polarization observables

We classify different kinds of measurement:

1. **Polarization of the outgoing particles is not measured**

   This means that the outgoing particles are unpolarized. This can be expressed by $\eta' = 0$, so that

   $$T_\eta^{\eta'} = T_\eta^0 \,. \tag{4.79}$$

   We have to distinguish between the following cases:

   - *Both incoming particles are unpolarized:*

     Then, we can write $\eta = 0$ and obtain

     $$T_\eta^{\eta'} = T_0^0 = 1 \,. \tag{4.80}$$

     This means, that the expectation value of the polarization $z_\eta^{\eta'}$ is identical to the unpolarized differential cross section $\overline{\frac{d\sigma}{d\Omega}}$, i.e. one sums over all polarization states.

   - *The incoming proton is polarized:*

     $$\eta = 1, q_p; 0, 0 \qquad \Rightarrow \qquad T_\eta^{\eta'} = T^0_{1,q_p;0,0} \tag{4.81}$$

- *The incoming deuteron is polarized:*

$$\eta = 0, 0; k_d, q_d \qquad \Rightarrow \qquad T_\eta^{\eta'} = T^0_{0,0;k_d,q_d}\,, \tag{4.82}$$

  where $k_d \in \{1, 2\}$.

- *Both incoming particles are polarized:*

$$\eta = 1, q_p; k_d, q_d \qquad \Rightarrow \qquad T_\eta^{\eta'} = T^0_{1,q_p;k_d,q_d} \tag{4.83}$$

2. **Polarization of one of the outgoing particles is measured**

   Here, we have to differentiate between the following cases:

   - *Both incoming particles are unpolarized:*
     Then, we can write $\eta = 0$ and obtain for
     - polarized outgoing triton

$$\eta' = 1, q_t; 0, 0 \qquad \Rightarrow \qquad T_\eta^{\eta'} = T_0^{1,q_t;0,0} \tag{4.84}$$

     - polarized outgoing radiation

$$\eta' = 0, 0; k_\lambda, q_\lambda \qquad \Rightarrow \qquad T_\eta^{\eta'} = T_0^{0,0;k_\lambda,q_\lambda} \tag{4.85}$$

   - *The incoming proton is polarized:*
     Then, we can write $\eta = 1, q_p; 0, 0$ and obtain for
     - polarized outgoing triton

$$\eta' = 1, q_t; 0, 0 \qquad \Rightarrow \qquad T_\eta^{\eta'} = T^{1,q_t;0,0}_{1,q_p;0,0}\,, \tag{4.86}$$

     - polarized outgoing radiation

$$\eta' = 0, 0; k_\lambda, q_\lambda \qquad \Rightarrow \qquad T_\eta^{\eta'} = T^{0,0;k_\lambda,q_\lambda}_{1,q_p;0,0} \tag{4.87}$$

   - *The incoming deuteron is polarized:*
     Then, we can write $\eta = 0, 0; k_d, q_d$ and obtain for
     - polarized outgoing triton

$$\eta' = 1, q_t; 0, 0 \qquad \Rightarrow \qquad T_\eta^{\eta'} = T^{1,q_t;0,0}_{0,0;k_d,q_d} \tag{4.88}$$

     - polarized outgoing radiation

$$\eta' = 0, 0; k_\lambda, q_\lambda \qquad \Rightarrow \qquad T_\eta^{\eta'} = T^{0,0;k_\lambda,q_\lambda}_{0,0;k_d,q_d} \tag{4.89}$$

- *Both incoming particles are polarized:*
  Then, we can write $\eta = 1, q_p; k_d, q_d$ and obtain for
  - polarized outgoing triton

$$\eta' = 1, q_t; 0, 0 \qquad \Rightarrow \qquad T_\eta^{\eta'} = T_{1,q_p;k_d,q_d}^{1,q_t;0,0} \tag{4.90}$$

  - polarized outgoing radiation

$$\eta' = 0, 0; k_\lambda, q_\lambda \qquad \Rightarrow \qquad T_\eta^{\eta'} = T_{1,q_p;k_d,q_d}^{0,0;k_\lambda,q_\lambda} \tag{4.91}$$

3. **Polarization of both of the outgoing particles is measured**

- *Both incoming particles are unpolarized:*

$$\eta = 0, 0; 0, 0 \qquad \Rightarrow \qquad T_\eta^{\eta'} = T_{0,0;0,0}^{1,q_t;k_\lambda,q_\lambda} \tag{4.92}$$

- *The incoming proton is polarized:*

$$\eta = 1, q_p; 0, 0 \qquad \Rightarrow \qquad T_\eta^{\eta'} = T_{1,q_p;0,0}^{1,q_t;k_\lambda,q_\lambda} \tag{4.93}$$

- *The incoming deuteron is polarized:*

$$\eta = 0, 0; k_d, q_d \qquad \Rightarrow \qquad T_\eta^{\eta'} = T_{0,0;k_d,q_d}^{1,q_t;k_\lambda,q_\lambda} \tag{4.94}$$

- *Both incoming particles are polarized:*

$$\eta = 1, q_p; k_d, q_d \qquad \Rightarrow \qquad T_\eta^{\eta'} = T_{1,q_p;k_d,q_d}^{1,q_t;k_\lambda,q_\lambda} \tag{4.95}$$

The symmetry properties lead to the reduction of the number of observables. In the following, we will successively discuss this.

4.6.2 Application of the symmetry properties

We will use the properties for hermiticity (4.76), for parity invariance (4.77), and for time reversal (4.78) to determine the dependences between the possible 36^2 polarization observables. It is important to emphasize, that we will use in all the following considerations the standard-center-of-mass-system as the frame of reference.

Due to the hermiticity condition, all observables are either real or imaginary. This fact and parity invariance provide:

$$\begin{array}{lll} T^{0,0;0,0}_{1,0;0,0} = 0 & \text{and} & T^{0,0;0,0}_{1,1;0,0} = T^{0,0;0,0}_{1,-1;0,0} \\ T^{0,0;0,0}_{0,0;2,1} = -T^{0,0;0,0}_{0,0;2,-1} & \text{and} & T^{0,0;0,0}_{0,0;2,2} = T^{0,0;0,0}_{0,0;2,-2} \end{array} \tag{4.96}$$

Using time reversal invariance yields:

$$\begin{array}{lll} T^{0,0;0,0}_{1,0;0,0} = T^{1,0;0,0}_{0,0;0,0} = 0 & \text{and} & T^{0,0;0,0}_{1,\pm1;0,0} = -T^{1,\pm1;0,0}_{0,0;0,0} \\ T^{0,0;0,0}_{1,q_p;1,q_d} = (-)^{q_p+q_d}\, T^{1,q_p;1,q_d}_{0,0;0,0} & \text{and} & T^{1,q_t;0,0}_{0,0;1,q_d} = (-)^{q_t+q_d}\, T^{0,0;1,q_d}_{1,q_t;0,0} \\ T^{0,0;0,0}_{0,0;2,q_d} = (-)^{q_d}\, T^{0,0;2,q_d}_{0,0;0,0} & \text{and} & T^{0,0;0,0}_{1,q_p;2,q_d} = (-)^{q_p+q_d}\, T^{1,q_p;2,q_d}_{0,0;0,0} \\ T^{0,0;2,q_\lambda}_{1,q_p;0,0} = (-)^{q_p+q_\lambda}\, T^{1,q_p;0,0}_{0,0;2,q_\lambda} & & \end{array} \tag{4.97}$$

Exploiting hermiticity results, that the observables

$$\begin{array}{lll} T^{0,0;0,0}_{1,q_p;0,0} & \text{and} & T^{0,0;0,0}_{0,0;1,q_d} \\ T^{0,0;0,0}_{1,q_p;2,q_d} & \text{and} & T^{0,0;2,q_\lambda}_{1,q_p;0,0} \end{array} \tag{4.98}$$

are imaginary and

$$\begin{array}{lll} T^{1,q_t;0,0}_{1,q_p;0,0} & \text{and} & T^{0,0;0,0}_{0,0;2,q_d} \\ T^{0,0;0,0}_{1,q_p;1,q_d} & \text{and} & T^{0,0;1,q_\lambda}_{0,0;1,q_d} \\ T^{0,0;1,q_\lambda}_{1,q_p;0,0} & \text{and} & T^{0,0;2,q_\lambda}_{0,0;2,q_d} \end{array} \tag{4.99}$$

are real. From parity invariance, one can conclude

$$\begin{array}{lll} T^{1,1;0,0}_{1,0;0,0} = -T^{1,-1;0,0}_{1,0;0,0} & \text{and} & T^{1,0;0,0}_{1,0;0,0} = -T^{1,0;0,0}_{1,-1;0,0} \\ T^{1,1;0,0}_{1,1;0,0} = T^{1,-1;0,0}_{1,-1;0,0} & \text{and} & T^{1,-1;0,0}_{1,1;0,0} = T^{1,1;0,0}_{1,-1;0,0} \end{array} \tag{4.100}$$

and by also taking into account time reversal invariance, one sees that

$$T^{1_t,1_t;0,0}_{1_p,0;0,0} = -T^{1_p,0;0,0}_{1_t,1_t;0,0}\,, \tag{4.101}$$

so that we obtain only four different proton-triton transfer coefficients. We provide the used quantum numbers with the indices of the corresponding particles whenever it is useful to clarify the relationships.
We obtain, furthermore, for the 15 components of the vector-tensor polarization coefficients only seven independent observables:

$$\begin{array}{ll} T^{0,0;2_\lambda,0}_{1_p,0;0,0} = 0 & T^{0,0;2_\lambda,1_\lambda}_{1_p,0;0,0} = T^{0,0;2_\lambda,-1_\lambda}_{1_p,0;0,0} \\ T^{0,0;2_\lambda,2_\lambda}_{1_p,0;0,0} = -T^{0,0;2_\lambda,-2_\lambda}_{1_p,0;0,0} & T^{0,0;2_\lambda,0}_{1_p,1_p;0,0} = T^{0,0;2_\lambda,0}_{1_p,-1_p;0,0} \\ T^{0,0;2_\lambda,1_\lambda}_{1_p,1_p;0,0} = -T^{0,0;2_\lambda,-1_\lambda}_{1_p,-1_p;0,0} & T^{0,0;2_\lambda,2_\lambda}_{1_p,1_p;0,0} = T^{0,0;2_\lambda,-2_\lambda}_{1_p,-1_p;0,0} \\ T^{0,0;2_\lambda,-1_\lambda}_{1_p,1_p;0,0} = -T^{0,0;2_\lambda,1_\lambda}_{1_p,-1_p;0,0} & T^{0,0;2_\lambda,-2_\lambda}_{1_p,1_p;0,0} = T^{0,0;2_\lambda,2_\lambda}_{1_p,-1_p;0,0} \end{array} \tag{4.102}$$

It follows that one can reduce the number of possible polarization observables to 25 observables. In the following section, we will show the calculation of six of them.

5 Calculation and Results

In this section we specify and present the differential cross section and six polarization observables at different energies for which we could find experimental data or other theoretical calculations. Then we will discuss the achieved results and show some peculiar effects we could observe. Furthermore, we will use these calculation as a comparison of three realistic potentials Bonn A, Bonn B and Paris. As two-body potentials, we use the EST parametrized version of the potentials by Haidenbauer [22] up to $j \leq 2$. in Section 5.9, we will illustrate the convergence of calculations by using different ranks of the partial waves in the EST-representation.

Besides, we will investigate the impact of the dipole ($E1$) and quadrupole ($E2$) contribution of the electromagnetic interaction. In all calculations meson exchange currents (MEC) are employed. Finally, it should be mentioned, that in all the following treatments Coulomb forces will not be considered.

First, we will state explicitly the representation of the mentioned six polarization observables.

5.1 Explicite representation of polarization observables

We introduce the common abbreviations in Table 1.

Observable	Notation	Coefficient
Vector analyzing power of **proton**	A_y	$\frac{i}{\sqrt{2}}\left(T^{00;00}_{11;00} + T^{00;00}_{1-1;00}\right)$
Vector analyzing power of **deuteron**	iT_{11}	$T^{00;00}_{00;11}$
Tensor analyzing power of **deuteron**	A_{yy}	$\frac{-\sqrt{3}}{2}\left(T^{00;00}_{00;22} + T^{00;00}_{00;2-2}\right) - \frac{1}{\sqrt{2}}T^{00;00}_{00;20}$
	T_{20}	$T^{00;00}_{00;20}$
	T_{21}	$T^{00;00}_{00;21}$
	T_{22}	$T^{00;00}_{00;22}$

Table 1: Polarization observables

It should be emphasized here, that experimental measurement data are only available for these listed observables. All calculated observables at $E_d = 10$ MeV are compared to data of the measurements by Goeckner, Pitts, and Knutson [46].

Using the shown method one can calculate the other possible observables. We will point out the numerical calculation of these six observables. First, we discuss the calculation of the cross section at different energies by employing different potentials.

5.2 Differential cross section of $p + d \to t + \gamma$

For the calculation of the differential cross section of the capture reaction, we apply equation (4.63). To describe the cross section in the photodisintegration reaction, one has to replace the factor $\frac{1}{6}$ by $\frac{1}{4}$ for the summation over possible spin states. The differential and total cross sections of photodisintegration and capture reaction are treated elaborately at different energies by Schadow in Ref. [5,8].

5.2.1 Potential dependence

Here, we want to point out the influence of different potentials on the differential cross section. We can see, that the curves in Figures 6 and 7 with BAEST ($j \leq 2$) are higher in the peak region because of the higher binding energy as discussed in Ref. [4,6].

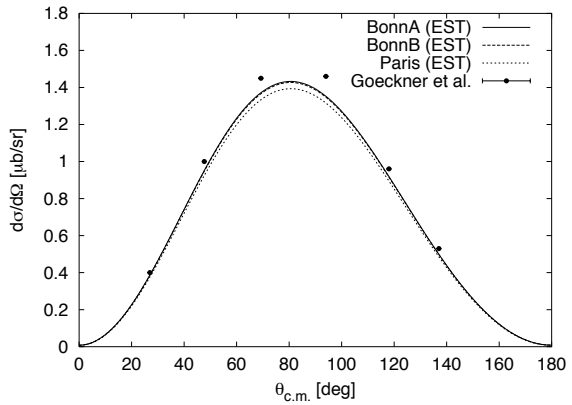

Figure 6: $\frac{d\sigma}{d\Omega}$ at $E_d = 10$ MeV with $E2$

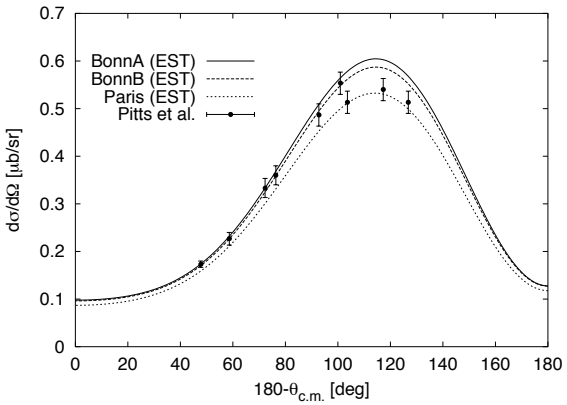

Figure 7: $\frac{d\sigma}{d\Omega}$ at $E_d = 95$ MeV with $E2$

We can see, that at $E_d = 95$ MeV the experimental data of Pitts et al. [47] are better covered by PEST in the peak region and by BBEST at the flanks. In the following, we will discuss the role of the binding energy.

5.2.2 Impact of the Binding energy

The differential cross section is usually expanded in terms of Legendre Polynomials

$$\sigma(\theta) = A_0 \left(1 + \sum_{k=1} a_k P_k(\cos\theta)\right) . \tag{5.1}$$

The factor A_0, which determine the peak height, depends on the binding energy given by the used potential. The following figures, where the differential cross section are divided by A_0, show the impact of employing higher partial waves on A_0 at different energies:

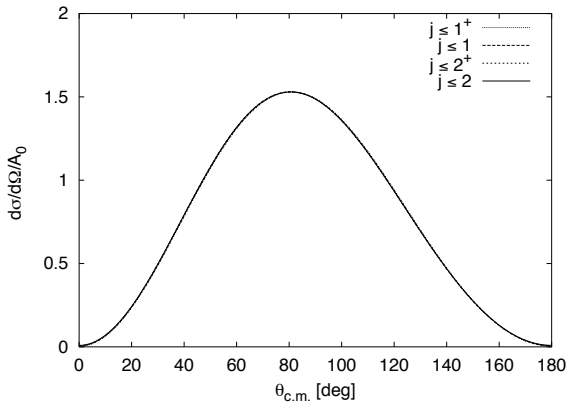

Figure 8: $E_d = 10$ MeV with BAEST and $E2$

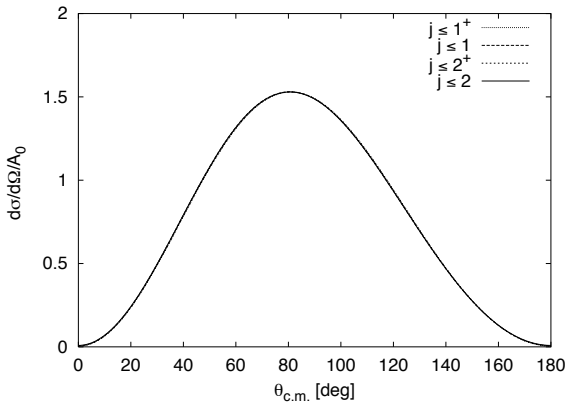

Figure 9: $E_d = 10$ MeV with BBEST and $E2$

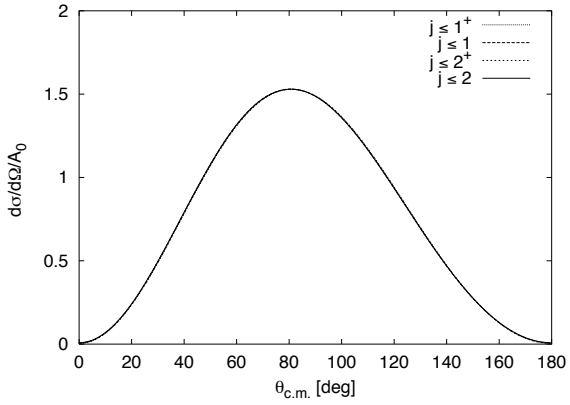

Figure 10: $E_d = 10$ MeV with PEST and $E2$

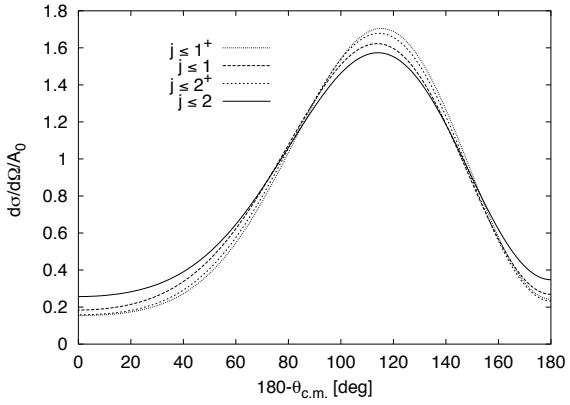

Figure 11: $E_d = 95$ MeV with PEST and $E2$

In all these figures, $E2$-contribution is taken into account. One sees for lower energies no difference between the employed limitations of the incorporated partial waves (further

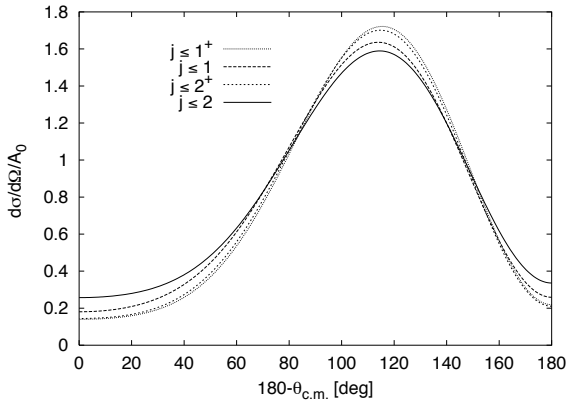

Figure 12: $E_d = 95$ MeV with BAEST and $E2$

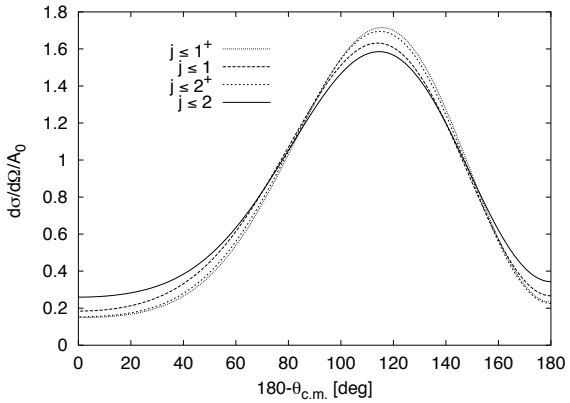

Figure 13: $E_d = 95$ MeV with BBEST and $E2$

details are presented in Table 2). For higher energies, it could be necessary to take higher partial waves to describe more accurately the experimental data.

Figures 14 and 15 demonstrate the relation between the triton binding energy and the peak height of the differential cross sections for different realistic potentials. We see that the chosen number of partial waves plays an crucial role, so that we can observe that the results for different potential with the same number of partial waves lie on a straight line.

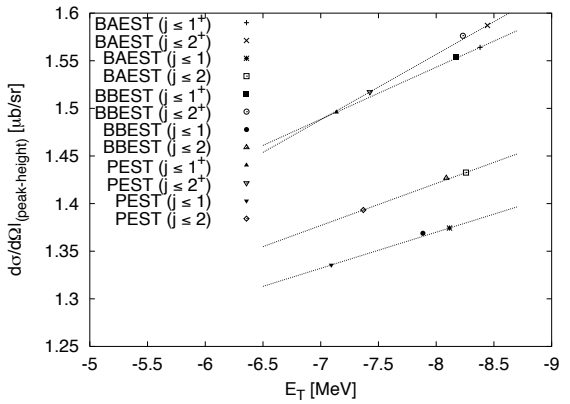

Figure 14: Correlation of peak heights and the binding energies at $E_d = 10$ MeV

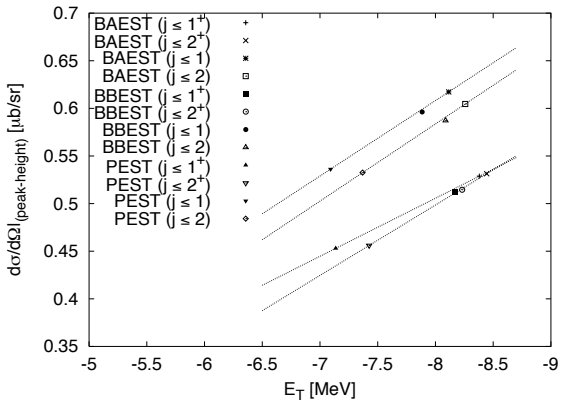

Figure 15: Correlation of peak heights and the binding energies at $E_d = 95$ MeV

The order of the straight lines is switched by taking higher energies. We can see a wider gap between the 5 and 9 channel and 10 and 18 channel calculations, i.e. using potentials with higher order of partial wave decomposition, in particular the p- and f-waves.

Similar Investigations by Schadow deliver, that there is one line for the s-wave MT I+III

potential and Yamaguchi potential with different parameters [6]. The resulting comparisons between the realistic and non-realistic potentials are treated by Sandhas et al. in Ref. [7]. There, it is exhibited that these potential investigations can not be used as an statement for the potentials about being "realistic" or "non-realistic".

5.2.3 $E2$-contribution

All the calculations above were done by taking into account $E2$. Now, we discuss the role of $E1$, $E1 + E2$ and the interference term. First calculations with realistic potentials are done by Heck [34]. The partly false calculations at $j \leq 1^+$ for the potential expansion are improved and extended to $j \leq 2$ by Schadow in Ref. [5].

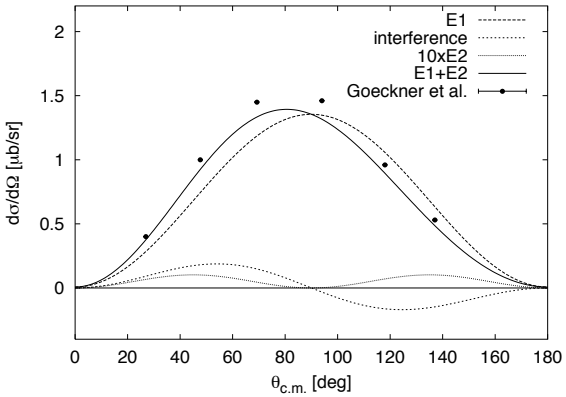

Figure 16: $E_d = 10$ MeV with PEST

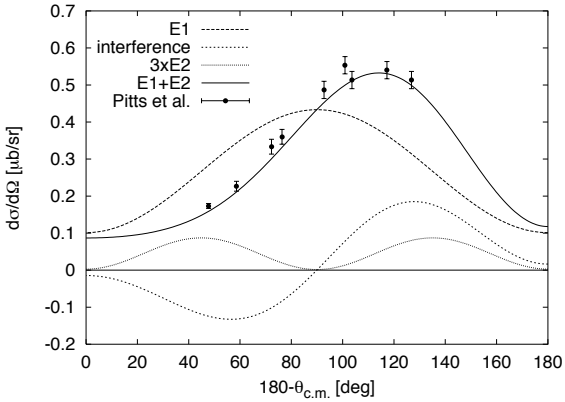

Figure 17: $E_d = 95$ MeV with PEST

The difference to $E1$ is that the isospin matrix elements of the interaction operator depend on the z-component. With this fact, we are able to differentiate between helium and triton. $E1$-transitions do not show this property.

Figures 16 and 17 illustrate that $E1$-contributions are several order of magnitude greater than $E2$. The interference term between $E1$ and $E2$ plays an important role. It is proportional to the product of the cross sections of $E1$ and $E2$ and to a combination of $\sin^2\theta\cos\theta$. It vanishes at an angle of 90°. Because of its peculiar distribution, it vanishes when the total cross section is to be calculated. Furthermore, the shifted sign of the distribution is remarkable.

5.3 Vector analyzing power of proton A_y

The experimental data unfortunately do not agree with our calculations as shown in Figures 18 and 20 for $E_d = 10$ MeV and in Figures 19 and 21 for $E_d = 95$ MeV (experimental data are taken from [46] and [47], respectively).

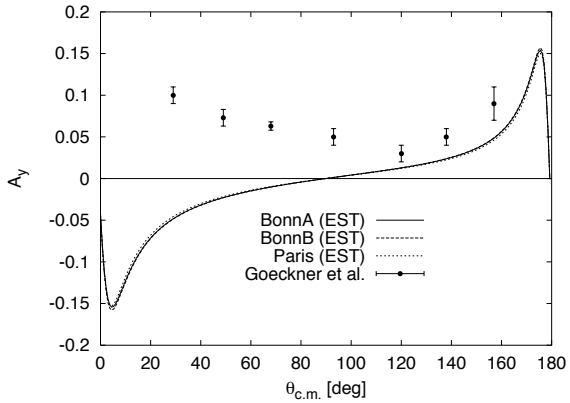

Figure 18: A_y at $E_d = 10$ MeV with $E2$

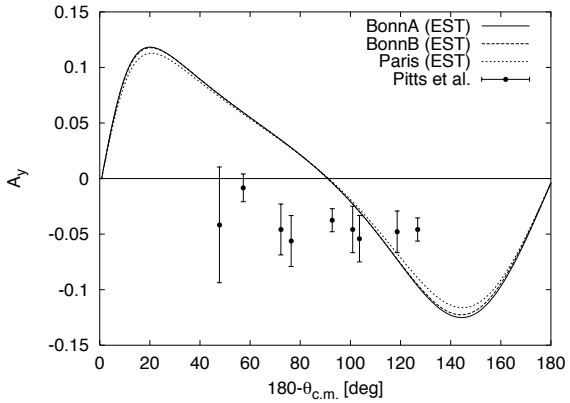

Figure 19: A_y at $E_d = 95$ MeV with $E2$

From the curves with only $E1$-contribution we can observe a symmetric form regarding to the origin of the coordinate system. The reflection point is shifted by taking into account $E2$-contribution. But as for the calculation of the differential cross section mentioned, this asymmetry is required to cover the data of the cross section and other observables in the following. As Fonseca and Lehman suggested in Ref. [9], employing the magnetic multipole contribution ($M1$) could improve the comparison with the the experimental data. Even by taking into account $E2$-contribution, we can not reach contenting results.

The available potentials do not indicate a significant difference for A_y, as shown in Figures 18 and 19. It is remarkable that these discrepancies are given for lower as well as higher energy range.

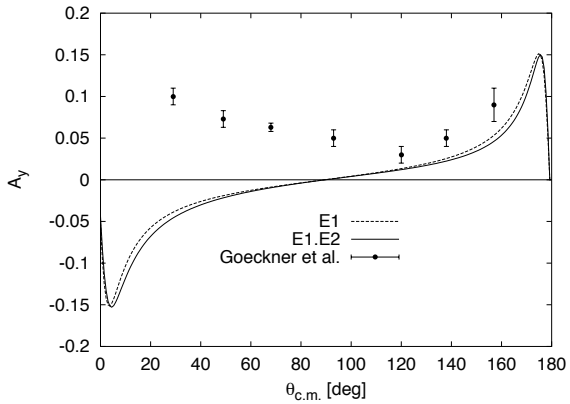

Figure 20: A_y at $E_d = 10$ MeV with PEST

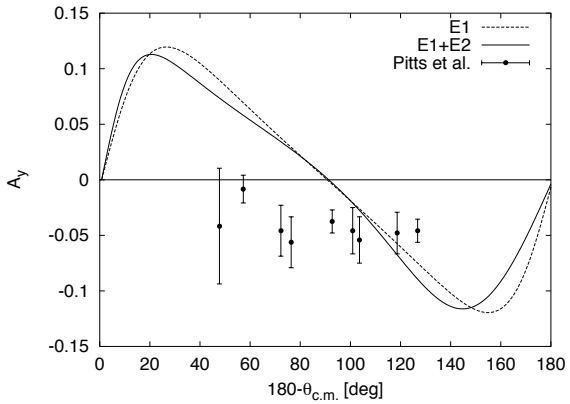

Figure 21: A_y at $E_d = 95$ MeV with PEST

5.4 Vector analyzing power of deuteron iT_{11}

As in the case of A_y, the calculations shown in Figures 22 and 23 do not agree with the data taken from the experiments done by Goeckner at al. [46]. The calculations of Fonseca an Lehman [9] by taking account of $E1$ do also not yield better agreement.

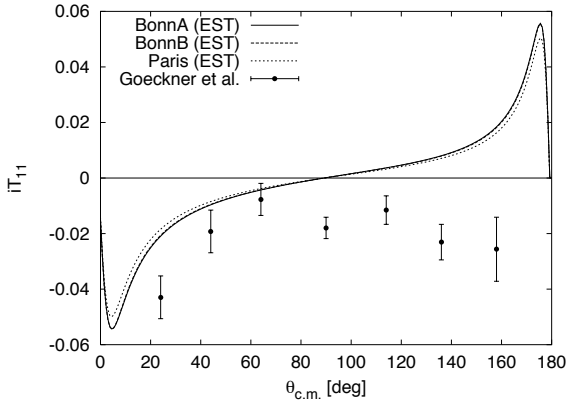

Figure 22: iT_{11} at $E_d = 10$ MeV with $E2$

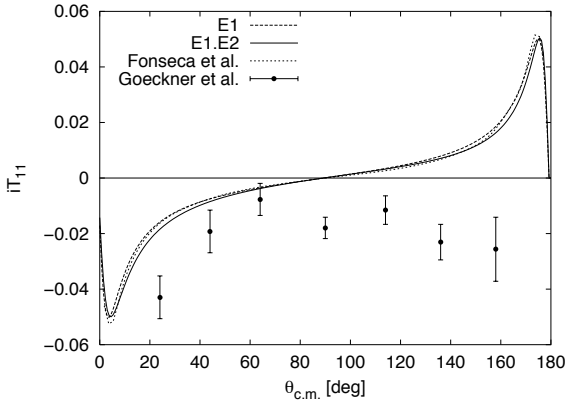

Figure 23: iT_{11} at $E_d = 10$ MeV with PEST

Even by taking account of $E2$-contribution, we can not achieve more contenting results at $E_d = 10$ MeV. As Fonseca, we suggest that the role of $M1$-contribution is not negligible.

This vector analyzing power iT_{11} does not provide a good test for different potentials, because Figure 22 shows no significant differences. Furthermore, we have observed a reflexion of the curves at the x-axis by calculating at higher energies (not illustrated). Unfortunately, there are no experimental data at higher energies available.

5.5 Tensor analyzing power of deuteron A_{yy}

The very exact measurement of A_{yy} done by Jourdan et al. [48] is well covered by our calculation as shown in the Figures 25 and 29. We can remark, that the curves up to the higher energies become more roundly. Since the error bars of the data set of Baumgartner et al. in Ref. [49] are too big, the experiment accuracy is questionable. We will discuss the phenomena of A_{yy}-calculations by their properties concerning the potential dependence and the $E2$-contribution.

5.5.1 Potential dependence

The difference between calculations with BAEST and BBEST in Figure 24 for $E_\gamma = 14.66$ MeV are visible first at extreme angles. We state this fact for $E_d = 29.2$ MeV in Figure 25 too, where the single measurement point is better covered by calculations with BAEST

and BBEST than with PEST.

The fact that the curves with BAEST and BBEST are indistinguishable in the interesting region is remarkable for other energies like $E_d = 45$ MeV and $E_d = 95$ MeV too, as shown in the Figures 26 and 27 (data of Ref. [50] and [47]).

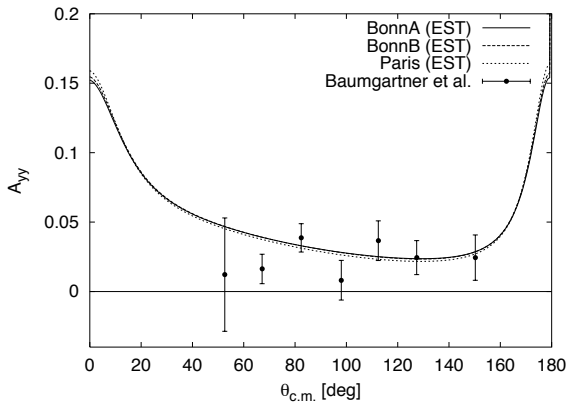

Figure 24: A_{yy} at $E_\gamma = 14.66$ MeV with $E2$

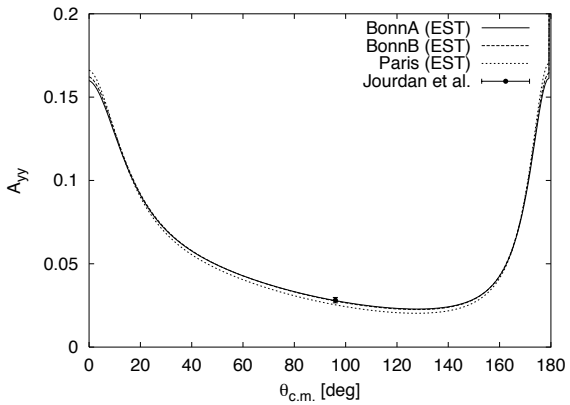

Figure 25: A_{yy} at $E_d = 29.2$ MeV with $E2$

We can notice, that the observable A_{yy} is not capable to test the quality of different potentials because of their insignificant influence. Besides the extreme angles, the curves for PEST runs lower than those with BAEST or BBEST.

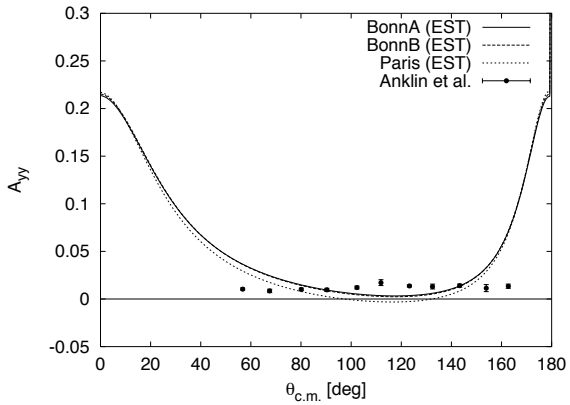

Figure 26: A_{yy} at $E_d = 45$ MeV with $E2$

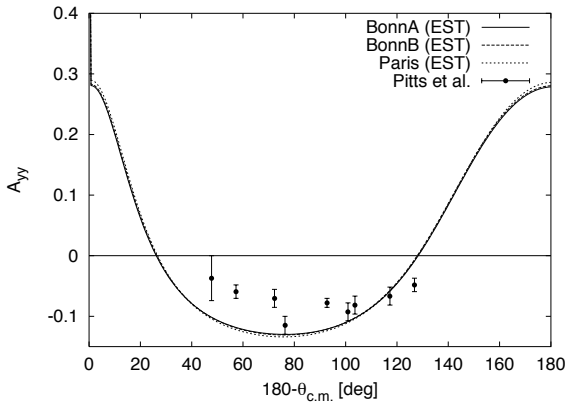

Figure 27: A_{yy} at $E_d = 95$ MeV with $E2$

5.5.2 Influence of the $E2$-contribution

The observed asymmetry of the cross sections caused by taking account of $E2$-contribution is visible by the A_{yy} curves, too, because of the relation for the cross section that enters in the definition of A_{yy}. That is why the curves are shifted to the higher angles. This asymmetry is clearly observable at all four calculated energies. It is necessary at $E_\gamma = 14.66$ MeV, as shown in Figure 28, whereas the accurate measurement at $E_d = 29.2$ MeV (Figure 29)is well covered by $E1$.

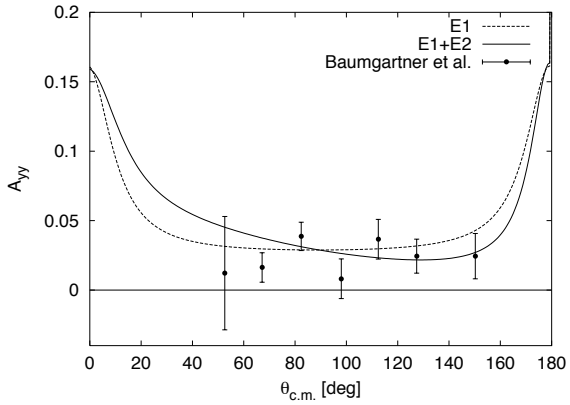

Figure 28: A_{yy} at $E_\gamma = 14.66$ MeV with PEST

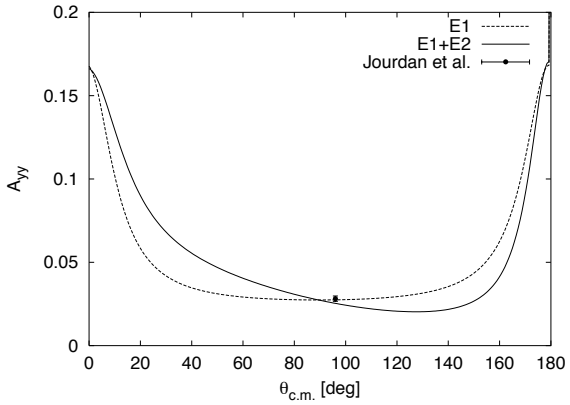

Figure 29: A_{yy} at $E_d = 29.2$ MeV with PEST

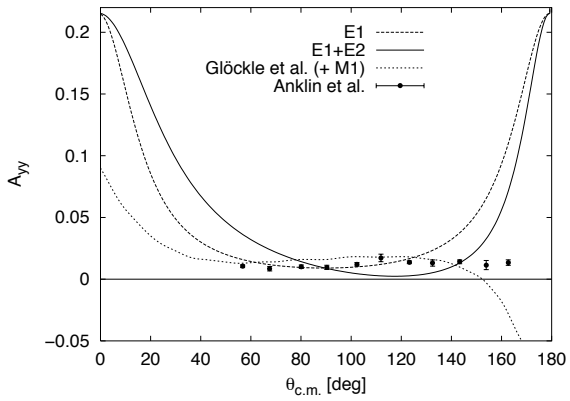

Figure 30: A_{yy} at $E_d = 45$ MeV with BBEST

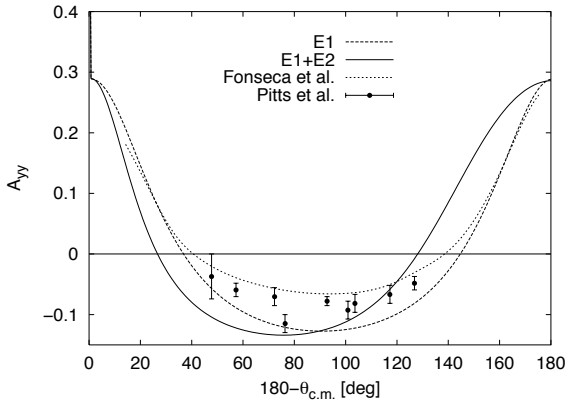

Figure 31: A_{yy} at $E_d = 95$ MeV with PEST

In the case of $E_d = 45$ MeV, where all measured points are on a almost straight line (see Figure 30), the agreement of our $E2$-calculations with the experimental data is not entirely satisfactory. Here, we can compare our curve to Glöckles two-dimensional calculation for the Bonn-B potential taking into account $M1$-contribution [50]. At the extreme angles, we

can observe considerable differences. Unfortunately, there are no measurement points at these angles for a satisfactory comparison. But the role of magnetic contributions seems to be significant at angles beyond 130°.

All measured points for $E_d = 95$ MeV are in the negative region as shown in Figure 31. Measurements between the energies 45 and 95 MeV could be helpful to point out the behavior at the transition between the positive and negative valued measured points. The theoretical calculation done by Fonseca and Lehman [9] yields a higher A_{yy}. One explanation for this discrepancy is the omitted coupling of $^3P_2$-$^3F_2$ partial waves in their calculations.

5.6 Tensor analyzing power of deuteron T_{20}

Here we can observe that all curves are in the negative region. Calculations at higher energies (e.g. $E_d = 95$ MeV) deliver positive values, but not at extreme angles. As in the previous figures, the asymmetry caused by taking account of $E2$-contribution is remarkable. The curves in Figure 32 run parallel for different potentials. The calculation with BAEST and BBEST cover best the data sets within the error bars.

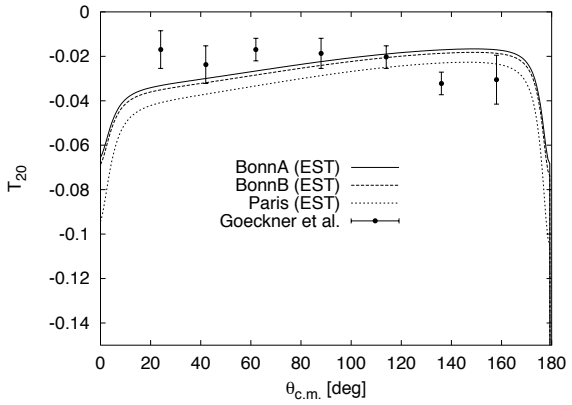

Figure 32: T_{20} at $E_d = 10$ MeV with $E2$

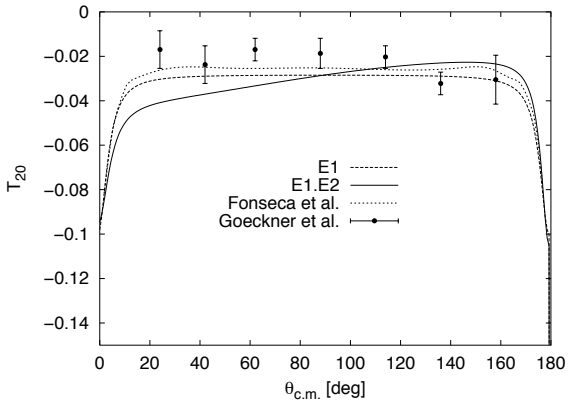

Figure 33: T_{20} at $E_d = 10$ MeV, PEST

As for A_{yy} mentioned, in Figure 33 the measured points are on an almost straight line, so that our $E2$-calculations do not deliver a satisfactory agreement. We observe no significant difference between the curve of Fonseca and Lehman [9] taking account of only $E1$ and our $E1$-calculation. This is also the case in Figure 35, where they took for some unknown reasons a lower energy than the experimental energy of the initial particle.
At the higher energy of $E_d = 19.8$, shown in Figure 34, we can remark no significant difference between the various potentials. They are different just at extreme angles. The influence of the $E2$-contribution is not remarkable. This is illustrated in the Figure 35 (data from Ref. [51]).

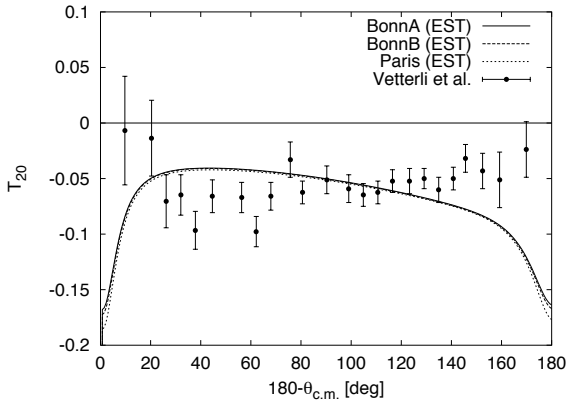

Figure 34: T_{20} at $E_d = 19.8$ MeV with $E2$

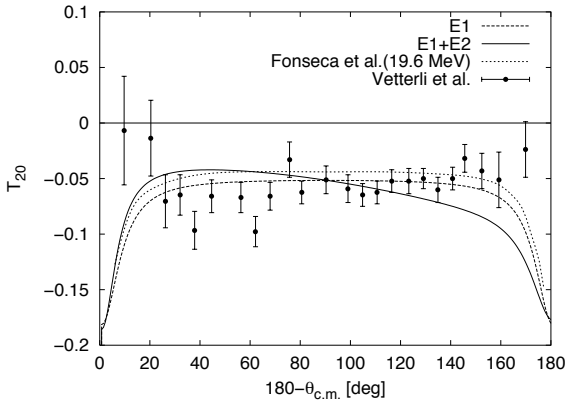

Figure 35: T_{20} at $E_d = 19.8$ MeV, PEST

The experimental data are increasing at the extreme angles, while our calculated curves show a decreasing behavior. Some of the points are discrepant to the rest of the data set, so that we can consider them as measurement errors. Furthermore, the width of some error bars points out an almost inaccurate measurement at $E_d = 19.8$ MeV.

5.7 Tensor analyzing power of deuteron T_{21}

The calculated curves cover very well the experimental data, specially by the choice of BAEST and $E1$, as shown in Figure 37. We can not remark any striking potential dependence in Figure 36.

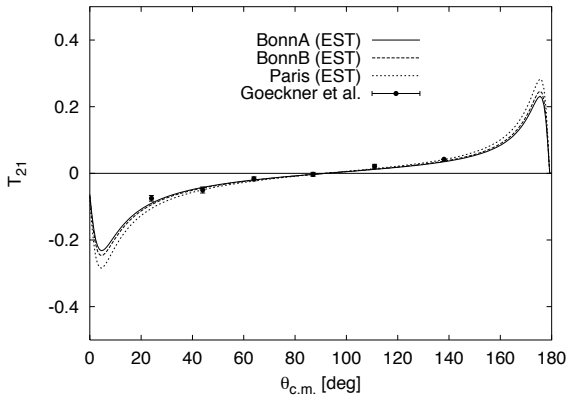

Figure 36: T_{21} at $E_d = 10$ MeV with $E2$

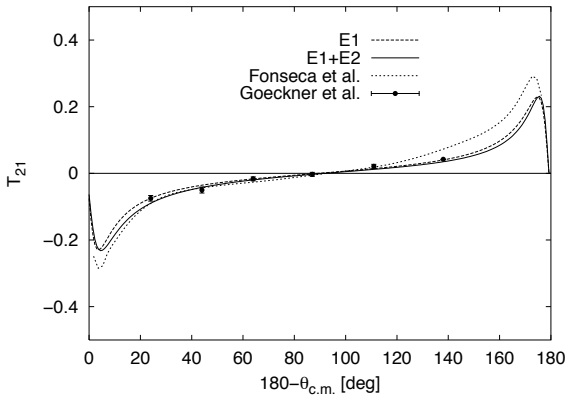

Figure 37: T_{21} at $E_d = 10$ MeV, BAEST

By rising the energies the maxima and minima are increased (not shown here). Unfortunately, there are no measurement points at extreme angles, so that we can not verify our results in this region. The $E1$-calculation for PEST of Fonseca and Lehman [9] do not

agree as well as our $E2$-curve for BAEST to the experimental data, as shown in Figure 37. One suggested reason of the wrong coupling has been mentioned above.

5.8 Tensor analyzing power of deuteron T_{22}

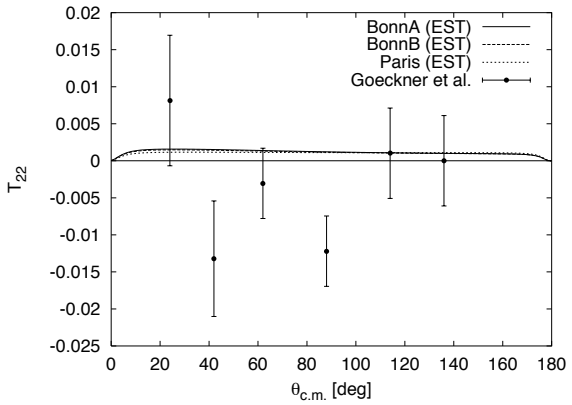

Figure 38: T_{22} at $E_d = 10$ MeV with $E2$

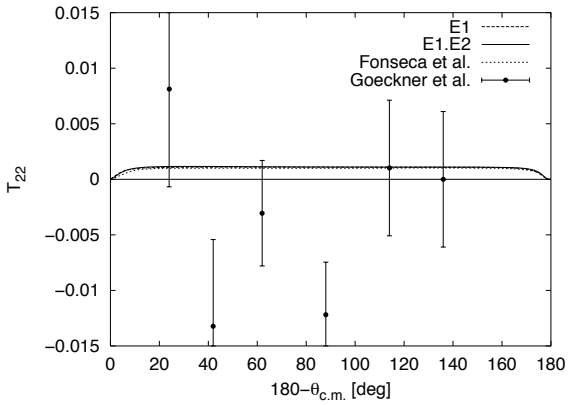

Figure 39: T_{22} at $E_d = 10$ MeV, PEST

As in the Figure 39 illustrated, there is neither the usual asymmetry caused by taking account of $E2$ remarkable nor any potential dependence in Figure 38. Therefor, T_{22} is not a good test neither for potential dependence nor for the influence of electric transition. Fonsecas and Lehmans $E1$-calculation for PEST confirm this result [9]. All curves are within the error bars, besides the measured points at $\theta = 42°$ and $88°$, which seem to be measuring errors.

5.9 Convergence

The calculated results above based on the EST representation. Now, we want to sketch the convergence by varying the rank in various two-body partial waves. We characterize these representations by $(n_1, n_2, n_3 \cdots)$, where $n_1, n_2, n_3 \cdots$ stand for ranks in the partial waves given in Table 2.

j	partial waves	*triton*	*FSI*
$j \leq 1^+$	$^1S_0$,$^3S_1$-$^3D_1$	5	26
$j \leq 1$	$^1S_0$,$^3S_1$-$^3D_1$,$^3P_0$,$^1P_1$,$^3P_1$	10	52
$j \leq 2^+$	$^1S_0$,$^3S_1$-$^3D_1$, $^1D_2$, $^3D_2$	9	56
$j \leq 2$	$^1S_0$,$^3S_1$-$^3D_1$,$^3P_0$,$^1P_1$,$^3P_1$, $^1D_2$, $^3D_2$, $^3P_2$-$^3F_2$	18	86

Table 2: Triton partial waves for different calculations

The third and forth column stand for the number of the employed channels.

Figure 40 demonstrate the fully converged calculations for the differential cross section at the low energy of $E_d = 10$ MeV employing the BAEST potential for a somewhat limited positive-parity two-body input ($j \leq 1^+$).

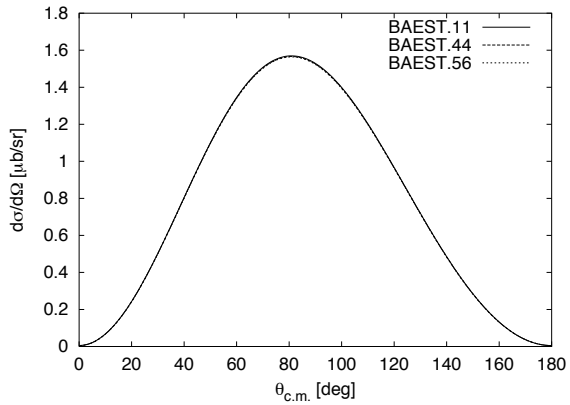

Figure 40: $\frac{d\sigma}{d\Omega}$ for BAEST ($j \leq 1^+$) at $E_d = 10$ MeV with $E2$

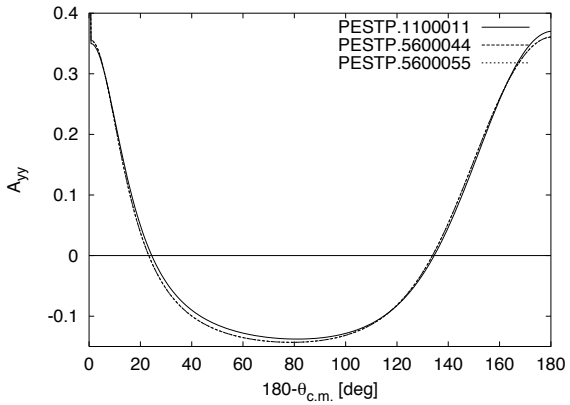

Figure 41: A_{yy} for PEST ($j \leq 2^+$) at $E_d = 95$ MeV with $E2$

We can also observe this convergence at higher energy of $E_d = 95$ MeV employing the PEST potential ($j \leq 2^+$). This convergence behavior demonstrate that for the cross section rank $= 1$ is sufficient, whereas for the polarization higher ranks are needed. On the other hand, it is not necessary to employ the highest available rank in partial waves.

6 Conclusions

As in Ref. [7] discussed, taking mesonic exchange currents (MEC) via Siegert's theorem involves an approximation. But, at least in the deuteron case it has been shown that the results obtained in this way fully agree with calculations based on a Hamiltonian which includes the MEC contributions explicitly [52] up to 100 MeV. In Ref. [5–8] it is shown that for cross section calculations taking account of MEC, FSI, and $E2$ leads to a satisfactory agreement with the experimental data sets. In this work, we could confirm these outcomes by calculating the polarization observables.

The presented curves for the various polarization observables demonstrate the dominance of the $E1$-contribution. Taking into account of $E2$ yields the necessary asymmetry. In Ref. [7] it was shown that the peak heights of the photodisintegration cross sections are correlated to the triton binding energy and that the chosen number of partial waves plays an crucial role. We could confirm this result for the inverse radiative capture reaction.

We have presented for T_{20}, T_{21}, A_{yy}, and the differential cross section excellent agreements to the experimental data sets at various energy ranges and employing different potentials. This achieved results insure a proper comparison of different potentials. The calculated cross sections, polarization observables, and peak heights, however, do not provide a sensitive test of the quality of the employed potentials in their EST representation. Thus, it should be emphasized that the EST method provide a sufficiently accurate approximation of the nucleon-nucleon potentials. The reduction of the original two-dimensional integral equations into a set of one-dimensional equations provides, therefore, quite accurate results. With this method the computational effort is considerably reduced. Taking account of higher partial waves, i.e., $j \leq 2$ stabilize the numerical results.

The big error bars for some observables, occurred for instance in figures 38 or 23, do not allow a real judgment, so that new, more accurate measurement would be needed. The discrepancies at the extreme forward and backward angles call for the calculation of $M1$-contributions.

A Rotation matrices

The quantities $D^j_{m'm}(\alpha,\beta,\gamma)$ are the standard rotation matrices defined through

$$\begin{aligned} D^j_{m'm}(\alpha,\beta,\gamma) &= \langle jm'|e^{-i\alpha j_z}\, e^{-i\beta j_y}\, e^{-i\gamma j_z}|\, jm\rangle \\ &= e^{-i\alpha m'}\, \langle m'|e^{-i\beta j_y}|m\rangle\, e^{-i\gamma m} \\ &= e^{-i\alpha m'}\, d^j_{m'm}(\beta)\, e^{-i\gamma m}\,, \end{aligned} \tag{A.1}$$

where (α,β,γ) are the Euler angles and $d^j_{m'm}(\beta)$ the reduced rotation matrices [38]. Because of the special rotational symmtery given by the capture reaction and the choice of the system of the coordinates, we use the rotation around the y-axis, whereby $\alpha = \gamma = 0$ and therefore

$$D^j_{m'm}(0,\beta,0) = d^j_{m'm}(\beta)\,. \tag{A.2}$$

For $j = \frac{1}{2}$ the elements of the reduced rotation matrix can be written as:

$$\begin{aligned} d^{\frac{1}{2}}_{\frac{1}{2},\frac{1}{2}}(\beta) &= \cos(\frac{\beta}{2}) & d^{\frac{1}{2}}_{\frac{1}{2},-\frac{1}{2}}(\beta) &= -\sin(\frac{\beta}{2}) \\ d^{\frac{1}{2}}_{-\frac{1}{2},\frac{1}{2}}(\beta) &= \sin(\frac{\beta}{2}) & d^{\frac{1}{2}}_{-\frac{1}{2},-\frac{1}{2}}(\beta) &= \cos(\frac{\beta}{2}) \end{aligned} \tag{A.3}$$

In the case of $j = 1$, one obtains for the reduced rotation matrix elements:

$$\begin{aligned} d^1_{1,1}(\beta) &= \frac{1}{2}\,(1+\cos(\beta)) & d^1_{1,0}(\beta) &= -\sqrt{\frac{1}{2}}\sin(\beta) & d^1_{1,-1}(\beta) &= \frac{1}{2}\,(1-\cos(\beta)) \\ d^1_{0,1}(\beta) &= \sqrt{\frac{1}{2}}\sin(\beta) & d^1_{0,0}(\beta) &= \cos(\beta) & d^1_{0,-1}(\beta) &= -\sqrt{\frac{1}{2}}\sin(\beta) \\ d^1_{-1,1}(\beta) &= \frac{1}{2}\,(1-\cos(\beta)) & d^1_{-1,0}(\beta) &= \sqrt{\frac{1}{2}}\sin(\beta) & d^1_{-1,-1}(\beta) &= \frac{1}{2}\,(1+\cos(\beta)) \end{aligned} \tag{A.4}$$

In the following, we list some useful relationships used in Section 4.3:

$$
\begin{aligned}
d^j_{m'm}(-\beta) = d^j_{mm'}(\beta) \qquad &; \qquad d^j_{m'm}(0) = \delta_{m'm} \\
d^j_{m'm}(\pi) = (-)^{j-m}\,\delta_{m'-m} \qquad &; \qquad d^j_{m'm}(\pi-\beta) = (-)^{j+m'} d^j_{m-m'}(\beta) \\
d^j_{m'm}(\beta) = (-)^{m'-m} d^j_{-m'-m}(\beta) \;&=\; (-)^{m'-m} d^j_{mm'}(\beta) \\
d^j_{m'm''}(\beta_1+\beta_2) \;&=\; \sum_m d^j_{m'm}(\beta_1)\, d^j_{mm''}(\beta_2)
\end{aligned}
\tag{A.5}
$$

For more detailed relations, we refer to [38].

References

[1] E. O. Alt, P. Grassberger, and W. Sandhas, *Reduction of the three-particle collision problem to multi-channel two-particle Lippmann-Schwinger equations*, Nucl. Phys. **B2**, 167 (1967).

[2] W. Sandhas, in *Few-Body Systems, Suppl. 1* (Springer-Verlag, Wien, 1986).

[3] B. F. Gibson and D. R. Lehman, *Two-body photodisintegration of ^3He and ^3H*, Phys. Rev. C **11**, 29 (1975).

[4] W. Schadow, W. Sandhas, J. Haidenbauer, and A. Nogga, *Comparison of triton bound state properties using different separable representations of realistic potentials*, submitted for publication .

[5] W. Schadow, *Behandlung der Photodesintegration von ^3H und ^3He mit Hilfe gekoppelter Integralgleichungen*, Doktorarbeit, Universität Bonn, 1997.

[6] W. Schadow and W. Sandhas, *Photodisintegration of the triton with realistic potentials*, Nucl. Phys. **A631**, 588c (1998).

[7] W. Sandhas, W. Schadow, G. Ellerkmann, L. L. Howell, and S. A. Sofianos, *Photodisintegration of three- and four nucleon systems*, Nucl. Phys. **A631**, 210c (1998).

[8] W. Schadow and W. Sandhas, *Radiative capture of protons by deuteron*, Phys. Rev. C **59**, 607 (1999).

[9] A. C. Fonseca and D. R. Lehman, *Full three-body calculation for $\vec{d} + p \to {}^3He + \gamma$ with realistic NN interaction*, Phys. Rev. C **48**, R503 (1993).

[10] S. Ishikawa and T. Sasakawa, *$p + \vec{d} \to {}^3He + \gamma$ reaction with realistic three-nucleon wave functions*, Phys. Rev. C **45**, R1428 (1992).

[11] W. Sandhas, *The three-body problem*, Acta Physica Austriaca Suppl. **IX**, 57 (1972).

[12] Th. Januschke, *Elastische Neutron-Deuteron-Streuung mit W-Matrix-Formulierung des 2-Teilchen-Inputs für das Paris-Potential*, Doktorarbeit, Universität Bonn, 1990.

[13] M. Lacombe, B. Loiseau, J. M. Richard, and R. Vinh Mau, *Parametrization of the Paris N-N potential*, Phys. Rev. C **21**, 861 (1980).

[14] R. Machleidt, K. Holinde, and Ch. Elster, *The Bonn Meson-Exchange Model for the Nucleon-Nucleon Interaction*, Phys. Rep. **149**, 1 (1987).

[15] R. Machleidt, in *Advances in Nuclear Physics*, edited by J. W. Negele and E. Vogt (Plenum Press, London, New York, 1989), Vol. 19, Chap. 2, p. 189.

[16] D. J. Ernst, C. M. Shakin, and R. M. Thaler, *Separable representation of two-body interactions*, Phys. Rev. C **8**, 46 (1973).

[17] D. J. Ernst, C. M. Shakin, and R. M. Thaler, *Separable representation of T matrices valid in the vicinity of off-shell points*, Phys. Rev. C **9**, 1780 (1974).

[18] J. Haidenbauer and W. Plessas, *Separable representation of the Paris nucleon-nucleon potential*, Phys. Rev. C **30**, 1822 (1984).

[19] J. Haidenbauer, Y. Koike, and W. Plessas, *Separable representation of the Bonn nucleon-nucleon potential*, Phys. Rev. C **33**, 439 (1986).

[20] J. Haidenbauer and Y. Koike, *Convergence of a separable expansion method in three-nucleon calculations*, Phys. Rev. C **34**, 1187 (1986).

[21] Y. Koike, J. Haidenbauer, and W. Plessas, *Nucleon-deuteron elastic scattering with the Paris nucleon-nucleon potential*, Phys. Rev. C **35**, 396 (1987).

[22] J. Haidenbauer, private communication.

[23] W. Schadow, J. Richter, and W. Sandhas, in *14th Int. IUPAP Conf. on Few-Body Problems in Physics* (CEBAF, F. Gross ed., Virginia, USA, 1994).

[24] A. C. Fonseca and D. R. Lehman, in *Proceedings of the 14th International IUPAP Conference on Few-Body Problems in Physics, Williamsburg, VA 1994,Ed. Franz Gross* (AIP, New York, 1995).

[25] I. M. Barbour and A. C. Phillips, *Photodisintegration of Three-Particle Nuclei*, Phys. Rev. Lett. **19**, 1388 (1967).

[26] Th. Januschke, T. N. Frank, W. Sandhas, and H. Haberzettl, *Neutron-deuteron scattering calculations with the Paris potential using the W-Matrix representation of the two-body input*, Phys. Rev. C **47**, 1401 (1993).

[27] T. N. Frank, H. Haberzettl, Th. Januschke, U. Kerwath, and W. Sandhas, *Neutron-deuteron breakup calculations with W-Matrix representation of the two-body input*, Phys. Rev. C **38**, 1112 (1988).

[28] T. Frank, *Neutron-Deuteron Aufbruchrechnungen mit Hilfe der W-Matrix-Methode*, Doktorarbeit, Universität Bonn, 1991.

[29] W. Glöckle, H. Witała, D. Hüber, H. Kamada, and J. Golak, *The three-nucleon continuum: achievements, challenges and applications*, Phys. Rep. **274**, 107 (1996).

[30] J. L. Friar, B. F. Gibson, and G. L. Payne, *Thermal $n-d$ radiative capture*, Phys. Lett. B **251**, 11 (1990).

[31] J. L. Friar, B. F. Gibson, G. Berthold, W. Glöckle, T. Cornelius, H. Witała, J. Haidenbauer, Y. Koike, , G. L. Payne, J. A. Tjon, and W. M. Kloet, *Benchmark solutions for a model three-nucleon scattering problem*, Phys. Rev. C **42**, 1838 (1990).

[32] A. Kievsky, M. Viviani, S. Rosati, D. Hüber, W. Glöckle, H. Kamada, H. Witała, and J. Golak, *Benchmark calculations for polarization observables in three-nucleon scattering*, Phys. Rev. C **58**, 3085 (1998).

[33] R. H. Landau, *Quantum Mechanics II* (Wiley, New York, 1996).

[34] Th. Heck, *Behandlung der Triton-Photodisintegration unter Berücksichtigung der E2-Übergänge*, Diplomarbeit, Universität Bonn, 1994.

[35] M. M. Gianini and G. Ricco, *Photoreactions above the Giant Dipole Resonances* (Springer, New York, 1985).

[36] A. J. F. Siegert, *Note on the interaction between nuclei and electromagnetic interaction*, Phys. Rev. **52**, 787 (1937).

[37] J. M. Eisenberg and W. Greiner, *Excitation Mechanisms of the Nucleus* (North-Holland, Amsterdam, 1970).

[38] A. Lindner, *Drehimpulse in der Quantenmechanik* (Teubner, Stuttgart, 1984).

[39] J. L. Friar and S. Fallieros, *Current conservation, exchange currents, and hadronic electromagnetic form factors*, Phys. Lett. **114B**, 403 (1982).

[40] The Madison Convention, in *Polarization Phenomena in Nuclear Physics*, edited by H. H. Barschall and W. Haeberli (The University of Wisconsin Press, Madison, 1970), p. XXV.

[41] M. Simonius, in *Polarization Phenomena in Nuclear Physics*, edited by H. H. Barschall and W. Haeberli (The University of Wisconsin Press, Madison, 1970), p. 401.

[42] R. K. Pathria, *Statistical Mechanics* (Pergamon Press, Oxford, 1977).

[43] M. Simonius, in *Polarization Nuclear Physics*, edited by D. Fick, Lecture Notes in Physics Vol. 30 (Springer-Verlag, Berlin-Heidelberg-New York, 1974), p. 38.

[44] B. A. Craver, Y. E. Kim, and A. Tubis, *Proton-deuteron radiative capture and the two-body photodisintegration of ^3He*, Nucl. Phys. **A276**, 237 (1977).

[45] C. B. Kuhl, *Integralgleichungs-Rechnungen zum Neutron-Deuteron-Streuproblem mit energieabhängiger Zweiteilchen-Wechselwirkung*, Doktorarbeit, Universität Bonn, 1996.

[46] F. Goeckner, W. K. Pitts, and L. D. Knutson, *Analyzing power measurements for $p-d$ radiative capture*, Phys. Rev. C **45**, R2536 (1992).

[47] W. K. Pitts, H. O. Meyer, L. C. Bland, J. D. Brown, R. C. Byrd, M. Hugi, H. J. Karwowski, P. Schwandt, A. Sinha, J. Sowinski, I. J. van Heerden, A. Arriaga, and F. D. Santos, *$^1H(\vec{\mathrm{d}},\gamma)^3He$ reaction at $E_\mathrm{d} = 95$ MeV*, Phys. Rev. C **37**, 1 (1988).

[48] J. Jourdan, M. Baumgartner, S. Burzynski, P. Egelhof, R. Henneck, A. Klein, M. A. Pickar, G. R. Plattner, W. D. Ramsay, H. W. Roser, I. Sick, and J. Torre, *$p - \vec{d}$ radiative capture and the ^3He d-state*, Phys. Lett. **162B**, 269 (1985).

[49] A. Arriaga and F. D. Santos, *^3He D effects in the $^1H(\vec{d},\gamma)^3He$ reaction*, Phys. Rev. C **29**, 1945 (1984).

[50] H. Anklin, L. J. dde Bever, S. Buttazzoni, W. G. abd J. Gloak, A. Honegger, J. Jourdan, H. Kamada, G. Kubon, Petijean, L. M. Qin, I. Sick, P. Steiner, H. Witała, M. Zeier, J. Zhao, and B. Zihlmann, *Tensor analyzing power A_{yy} of $\vec{\mathrm{d}}$-p radiative capture*, Nucl. Phys. **A636**, 189 (1998).

[51] M. C. Vetterli, J. A. Kuehner, A. J. Trudel, C. L. Woods, R. Dymarz, and A. A. Pilt, *Measurement of T_{20} for the reaction $^1H(d_\mathrm{pol},\gamma)$ ^3He and D-state effects in ^3He*, Phys. Rev. Lett. **54**, 1129 (1985).

[52] H. Arenhövel and M. Sanzone, *Photodisintegration of the Deuteron (Few-Body Systems Suppl. 3* (Springer-Verlag, Wien, 1991).

Danksagung

Herrn Prof. Dr. W. Sandhas möchte ich dafür danken, daß ich mich mit diesem interessanten Thema befassen und dadurch vieles lernen konnte. Vor allem möchte ich seinen Einsatz erwähnen, der die ausgezeichnete Zusammenarbeit mit Herrn Dr. Wolfgang Schadow – und nicht zuletzt eine mehrwöchige USA-Reise – ermöglichte.

Herrn Dr. Wolfgang Schadow gilt mein besonders herzlicher Dank, nicht nur für seine wissenschaftliche Unterstützung und seinen unermüdlichen Einsatz, sondern auch für die menschliche Bereicherung. Seiner Frau Jutta Trömpert möchte ich vor allem für die schönen Wochen in Athens/Ohio danken.

Herrn Dr. Andreas Wißkirchen danke ich für seine Hilfsbereitschaft bei Computerproblemen. Herrn Nicolas Janberg, Matthias Niemeyer und Frau Petra Schmidt danke ich für das Korrekturlesen. Auch den anderen Mitgliedern des Instituts möchte ich für die vielen kleinen und großen Hilfestellungen, die interessanten Gespräche und vor allem das freundliche Arbeitsklima danken. Dabei möchte ich vor allem Frau Patricia Zündorf erwähnen. Herrn Martin Weber danke ich für die geistreiche und nette gemeinsame Zeit.

Nicht zuletzt möchte ich mich bei meiner Familie bedanken, die mir das Studium ermöglicht hat, sowie bei allen, die dafür gesorgt haben, daß es neben der Physik auch andere Dinge gibt, die mein Leben mit noch mehr Freude bereichern.